Aus dem Institut für Zahn- Mund- und Kieferheilkunde
der Medizinischen Fakultät Charité – Universitätsmedizin Berlin

DISSERTATION

Assessing the degradation behavior of magnesium alloys using electrochemical methods

Beurteilung des Abbauverhaltens von Magnesiumlegierungen mit elektrochemischen Methoden

zur Erlangung des akademischen Grades
Doctor medicinae dentariae (Dr. med. dent.)

vorgelegt der Medizinischen Fakultät
Charité – Universitätsmedizin Berlin

von

Yuqiuhan Zhang

aus Henan, China

Datum der Promotion: 03.03.2023

Table of Contents

List of abbreviations

Abbreviation	English full name
HER	Hydrogen evolution reaction
HE	Hydrogen evolution
EC	Electrochemical
MEM	Minimum Essential Medium
HBSS	Hanks` Balanced Salt solution
OCP	Open circuit potential
SEM	Scanning Electron Microscope
Mg XHP	Mg extremely high pure
BMs	Biometals
CV	Cyclic voltammetry
NHE	Normal hydrogen electrode

Abstract

Introduction: Magnesium, a biodegradable biomaterial, has the potential to be applied in dental implantology as a bone augmentation material. The electrochemical characterization of the surface allows us to trace the deterioration process in vivo. The difficulty is to estimate the deterioration rate from the measurement data in order to predict the component's "lifetime". The formation of local elements should be avoided, ideally evenly distributed, so that a degradation takes place from the outside to the inside. This should ensure that the degradation of the Mg structure takes place as far as possible at the rate at which the bone is newly formed. The aim of the work was to carry out a more detailed evaluation of the degradation behavior on different Mg samples by microscopic observation of the surface during the electrochemical measurement.

Methods: Setting up an optical-electrochemical cell chamber with magnesium and magnesium alloys in electrochemical corrosion measurements. Observing and recording the surface degradation process under microscope. At 37°C, specimens were examined in several circulating electrolytes, including MEM, HBSS, and MEM+ (MEM supplemented with $NaHCO_3$). CV was measured followed by cycle polarization, which was then repeated previous steps after 30mins. Thus, it is possible to observe and correlate surface processes such as hydrogen evolution and oxide deposition in real time with electrochemical data. The electrochemistry data, which included the OCP exchange current density(i_0) and corrosion potential, were compared to the potential changes that occurred over time throughout these treatments. They were computed in this instance using R_P obtained from linear polarization and an estimate of the Stern–Geary constant. Additionally, the linear polarization curve and EC exchange current corrosion value are used to determine how magnesium and magnesium alloys evolve throughout the corrosion process.

Result: The corrosion behavior of pure Mg and MgXAg alloys differs significantly. Adding Ag to magnesium standardizes electrochemical activity and hence deterioration independent of test medium. After the tests, the video microscopic movies indicate comparable corrosion and deterioration in CO_2-containing electrolytes. Throughout OCP measurements, the surface develops distinctive patches that remain stable even during CV.

Conclusion: Video microscopic observation of the degradation of Mg and Mg alloys raises a variety of new questions for assessing the degradation. The question of how the Ag additives act in the Mg alloy and act as possible hydrogen development spots can currently only be suspected. Further investigations are necessary to find an answer to these and other questions. For this purpose, strategies for image evaluation still have to be developed, which allow, among other things, an effective determination of the electrochemically active surface.

Zusammenfassung

Einleitung: Magnesium, ein biologisch abbaubares Biomaterial, hat das Potenzial, in der dentalen Implantologie als Knochenaufbaumaterial verwendet zu werden. Mit Hilfe der elektrochemischen Charakterisierung der Oberfläche ist es möglich, den Degradationsprozess so zu verfolgen, wie er auch in-vivo abläuft. Die Herausforderung besteht darin, aus den Messdaten die Degradationsgeschwindigkeit so zu bestimmen, dass eine verlässliche Prognose für die „Lebenszeit" des Bauteils möglich wird. Es sollte die Bildung von Lokalelementen vermieden werden, idealerweise also gleichmäßig verteilt, so dass ein Abbau von außen nach innen erfolgt. So sollte sichergestellt werden, dass der Abbau der Mg-Struktur möglichst mit der Geschwindigkeit erfolgt, mit der der Knochen neu gebildet wird.

Methoden: Aufbau einer optisch-elektrochemischen Zelle für elektrochemische Korrosionsmessungen an Magnesium und Magnesiumlegierungen. Beobachtung und Aufzeichnung des Oberflächenveränderungen unter dem Videomikroskop. Bei 37 °C wurden die Proben in verschiedenen, zirkulierenden Elektrolyten untersucht, darunter MEM, HBSS und MEM+ (MEM ergänzt mit $NaHCO_3$). Zuerst wurde der OCP gemessen, dann ein CV und dann nach 30 Minuten eine Wiederholung der gleichen Schritte. Somit war es möglich, Oberflächenprozesse wie Wasserstoffentwicklung und Oxidabscheidung in Echtzeit zu beobachten und mit elektrochemischen Daten zu korrelieren. Die elektrochemischen Daten, OCP, Austauschstromdichte i_0 und das Korrosionspotential, wurden für die Bewertung der Degradation herangezogen. I_0 als Maß für die Degradationsgeschwindigkeit wurden in diesem Fall unter Verwendung von R_P und der Stern-Geary-Konstante aus den verschiedenen CV berechnet. Der Mittelwert und die Standardabweichung sind in den Tabellen im Ergebnisteil zusammengefasst.

Ergebnisse: Die Ergebnisse zeigen, dass es deutliche Unterschiede im Korrosionsverhalten zwischen den reinen Mg Proben und den MgXAg Legierungen gibt. Die Zugabe von Ag zu Magnesium führt zu einer Vereinheitlichung der elektrochemischen Aktivität und somit des Abbaus unabhängig vom gewählten Testmedium. Die videomikroskopischen Aufnahmen zeigen am Ende der Messungen in den CO_2 haltigen Elektrolyten ähnliche Korrosions- respektive Degradationsspuren.

Während der Zeit der OCP Messungen zeigen sich schon erste charakteristische Spots auf der Oberfläche, die auch während der CV sich nicht verändern.

Schlussfolgerung: Die videomikroskopische Beobachtung der Degradation von Mg und Mg-Legierungen wirft eine Vielzahl neuer Fragen zur Beurteilung der Degradation von Mg- und Mg-Legierungen auf. Die Frage wie die Ag Zusätze in der Mg Legierung agieren und als mögliche Wasserstoffentwicklungsspots fungieren kann momentan nur vermutet werden. Hier sind weiter Untersuchungen notwendig, um auf diese und andere Fragen eine Antwort zu finden. Hierzu müssen noch Strategien zur Bildauswertung entwickelt werden, die u.a. eine effektive Bestimmung der elektrochemisch aktiven Oberfläche erlauben.

(Diese Zusammenfassung wird mit Genehmigung der MDPI-Verlagsgruppe wiederveröffentlicht. Es ist Teil der folgenden Veröffentlichung: Yuqiuhan Zhang, Tycho Zimmermann, Wolf-Dieter Mueller, Frank Witte, Florian Beuer, Andreas Schwitalla. Exploring the degradation behavior of MgXAg alloys by in vitro electrochemical methods. Bioactive Materials, 2021, ISSN 2452-199X, https://doi.org/10.1016/j.bioactmat.2021.05.044.)

Synopsis

Utilizing electrochemical techniques to observe the corrosion process on the surface of magnesium metal and its alloys to investigate the relationship between pitting corrosion and electrochemical data.

1. Introduction

As innovative biomaterials for bone grafting therapy, biodegradable metals are being considered[1]. In using magnesium as implant material magnesium, a variety of beneficial qualities are attributed: low density, possibility of the manufacturing of small structures, ease of manipulation, the properties of the breakdown products of magnesium (Mg^{2+} ions) to encourage calcium and phosphorus deposition and compact bone formation[2]. Its full breakdown and absorption make a second (removal) surgery unnecessary, for instance when employed for the purpose of osteosynthesis[3].

Magnesium is more highly reactive than other biodegradable metals, such as zinc or iron. The fast degradation in the humid physiology remains a key obstacle to wide-ranging use since magnesium-based implant structural failure can lead to rapid mechanical failure of the bone, before it is structurally healed[4], [5].

Magnesium and magnesium alloys deteriorate in a non-uniform manner [6]. This is owing to a complicated degradation behavior caused by galvanic coupling, which occurs when the anodic and cathodic partial reactions of a redox-reaction system occur on the same surface area [7]. As a result of the anodic reaction (1), one portion of the surface in contact with the electrolyte (the body fluid or simulated body fluid) is oxidized and deteriorated, while the two electrons are transported to the cathodic partial reaction, where hydrogen evolution (HE) occurs (2). The hydrogen evolution process (HER) is the primary cathodic reaction that occurs spontaneously during magnesium corrosion. Additionally, the process consumes H^+ ions, resulting in a rise in the concentration of OH^- ions (3) and an increase in the pH of the physiological electrolyte, precipitating magnesium phosphate and carbonate[8]. The dissolved Mg^+ and OH^- ions then precipitate as a magnesium hydroxide layer on the surface of the magnesium or magnesium alloys (4) [6], [8].

$Mg \rightarrow Mg^{2+} + 2e^-$ (anodic partial reaction) (1)

$2H_2O + 2e^- \rightarrow H_2O + H_2\uparrow$ (cathodic partial reaction) (2)

$Mg + 2H_2O \rightleftharpoons Mg^{2+} + 2OH^- + H_2\uparrow$ (overall reaction) (3)

$Mg^{2+} + 2OH^- \rightarrow Mg(OH)_2$ (product formation, hydroxide layer) (4)

$Mg(OH)_2 + 2Cl^- \rightarrow MgCl_2 + 2OH^-$ (5)

Humans have utilized silver for thousands of years because of potent antibacterial properties. Silver containers were being used to hold drinks and food during Alexander the Great's reign [9]. Bulk silver in vessels and coins has given way to ionic silver enhanced with silver salts (such as $AgNO_3$) or adsorbed on carrier materials, and so has the usage of silver in jewelry and watches. [9]–[11]. As silver is considered to be of low toxicity in the human body. It is anticipated that clinical exposure to silver via inhalation, ingestion, topical application, urological or hematogenous routes would provide low risk [12]. As a bone implant material, binary magnesium–silver alloys have been created to give antibacterial properties to biodegradable magnesium and also be biocompatible. When coupled with its proclivity for degradation under physiological circumstances, the antibacterial characteristic may be retained throughout the implant's life. Among the parameters for evaluating biocompatibility and antibacterial activity [13], the corrosion rates and phases affect the corrosion process [14]. By adding silver, the corrosion potential of Mg–Ag metal complexes is changed anodically. Due to the essential nature of these complicated interactions, it is necessary to thoroughly investigate the corrosion behavior of magnesium-silver alloys [15]–[17].

While cell-based studies are done in physiological conditions, the environment has a significant effect on the degrading behavior of many materials. This is not only for biodegradable metals (magnesium, iron, zinc, and tungsten), but also for biodegradable polymers. As noted in a major essay [4], even when evaluating materials in general, physiological circumstances should be used, such as replicated bodily fluids. This is especially more fascinating in the case of biodegradable materials, as a constantly changing interface between the substance and the cells develops over time. Understanding this evolution is critical in this field of inquiry. Additionally, biological hints (e.g. cellular communication, interaction of diverse cell types, material protein interactions) must be analyzed, as they will have an effect on material degradation [18]. Numerous types of simulated bodily fluids were utilized in *in vitro* tests to investigate the biodegradation of magnesium and magnesium alloys. There is still no apparent consensus about the optimal setting for simulating physiological *in vivo* circumstances [16]. Mg is corroded in the human body by 0.14 M NaCl solution and a trace quantity of other inorganic compounds (such as Ca2+, PO43-, and HCO3-) [19]. Blood has a typical pH of 7.4, typically maintained via the CO2/HCO3- system [20]. Chloride ions typically accelerate corrosion [21] owing to the fact that the generation of $MgCl_2$ promotes the release of OH^- ions from

the precipitation layer (5), which may react with the dissolved Mg^{2+}ions Phosphates and carbonates, on the other hand, have the capacity to encourage the formation of corrosion products that are protective or partly protective [12]. Organic components, such as proteins, organisms, or bacteria, might further complicate the corrosion reaction [22], [23]. Also because solubility of calcium phosphate is also temperature sensitive, the body temperature of 37°C may both accelerate and modify the corrosion reaction when compared to room temperature [22]. These numerous influencing elements derived from the body environment complicate research on the corrosion process.

In new findings, biometals (BMs) such as Magnesium, Zinc and Iron have all been proven to have positive impacts on bone regeneration. As beginning, we select and compare the electrochemical degradation processes of 10 frequently used metals which are nontoxic and harmless in daily life (Zinc, Yttrium, Copper, Iron, Tungsten, Cobalt, Molybdenum, Zirconium, Tin and Nickel)[22], [24]–[27]. Expect to serve as a guideline for the next generation of magnesium improvements. Recent studies published in the literature have shown clearly that magnesium consumption is unique in terms of its electrochemical activity when compared to other nutrients. Corrosion of magnesium and its alloys occurs naturally as an electrochemical reaction, and their electrochemical behavior ultimately determines its corrosion performance or attributes. Identifying the electrochemical processes that occur throughout the corrosion process can offer a theoretical foundation for understanding the corrosion phenomena associated with magnesium and its alloys [22], [28]. Thus, the purpose of this work was to connect electrochemical (EC) measurements with a video-microscopic observation of surface changes over time under the influence of three different electrolytes derived from the cell culture mediums HBSS and MEM, in order to more accurately anticipate the degradation process.

2. Materials and Methods

MEM (Biochrom GmbH, Germany) and HBSS (Life Technologies Limited, UK) buffers were used in these studies since they are frequently used and recommended in the literature. In comparison to MEM, which includes extra amino acids and vitamins, HBSS contains increased $NaHCO_3$ (Sigma-Aldrich Chemie GmbH, Germany), as indicated in Table 1. To provide for a more accurate comparison of the corrosion process, 0.35g/L sodium bicarbonate was added to the MEM Plus group.

Table.1: The major components of MEM, HBSS and MEM plus (formulations offered by manufacturer)[29].

	MEM (g/L)	HBSS (g/L)	MEM Plus (g/L)
NaCl	6.8	8	6.68
$CaCl_2$	0.2	0.14	0.2
KCl	0.4	0.4	0.4
$CaCl_2$	0.2	0.14	0.2
$MgSO_4$	0.97	0.098	0.2
NaH_2PO_4	0.14	0.06	0.14
Special additives	w/o Phenol red Vitamins Amino acids w/o$NaHCO_3$	w/o Phenol red w/o Amino acids $NaHCO_3$ 0.35 KH_2PO_4 0.06 $MgCl_2$ 1.0	w/o Phenol red Vitamins Amino acids +0.35g/L $NaHCO_3$

Table.2: The information of 10 commonly used biometal materials.

Material	**Quality**	**Deliver**
Cobalt	99.99%	Aldrich Chemical Company
Copper	99.98%	Aldrich Chemical Company
Iron	99.9+%	Aldrich Chemical Company
Molybdenum	99.9+%	Aldrich Chemical Company
Nickel	99.997%	Aldrich Chemical Company
Tin	99.999%	Aldrich Chemical Company
Tungsten	99.9+%	Aldrich Chemical Company
Yttrium	99.90%	Aldrich Chemical Company
Zinc	99.9985%	Alfa Aesar
Zirconium	99.9+%	Aldrich Chemical Company

Mg XHP (purity: 99.99%) and Mg pure (purity: 99%) as well as three Mg-Ag alloys - Mg2Ag, Mg4Ag, and Mg6Ag - which contain 1.87%, 3.82%, and 6.00% silver and 98%,

96%, and 94% magnesium, were cast and treated with solution T4 respectively. All specimens were cylindrical, measuring 10mm in diameter and 5mm in thickness. An optical coupled electrochemical measuring setup was utilized to characterize the early deterioration process during 2 hours 10 mins [30].

2.1 Preparation of Magnesium specimens

Mg XHP, Mg pure, and MgXAg (X=2,4,6) samples were produced by partially encapsulating the sample in an epoxy resin to prevent it from crumbling during grinding. The surface was ground from 800 to 2500 using silicon carbide sandpaper (150mm Hermes, Germany), then polished with 1.0 m silica suspension and etched for 10 seconds with a solution mainly composed of glacial acetic acid and picric acid. Following that, the specimens' surfaces were cleaned with ethanol and dried.

2.2 Roughness measurement

To compare the surface conditions of the specimens, a video microscope (Keyence VHX-5000, Japan) was used to view them, and an IF-microscope was used to quantify the roughness at five points on each specimen (Alicona, Austria). The magnifying optic is IFM G4 10x/0.30A. Vertical scanning and calibration coordinate system used before measurements. The measurements took 5 fields of view(left, right, up, down and middle) separately. Taking the average value for comparison.

2.3 Electrochemical measurements

The specimens were linked on their reverse side to a copper wire through a silver amalgam for electrochemical tests. The surface reactions of specimens were examined using a video microscope (Keyence VHX-5000) connected to a specialized electrochemical cell [31], as shown in (Fig.1). PStrace (PalmSens, Netherlands) was used to modify and aggregate the electrochemical data in conjunction with a mini-potentiostat (Emstat3+, PalmSens, Netherlands). The potentials are related to SCE (saturated calomel electrode) +0.241V vs NHE (Normal hydrogen electrode).

Using a laboratory pump, the liquids were pushed through the apparatus (Watson Marlow 5050Di, United Kingdom). The flow rate was set at 4.3ml/min and the temperature to 37°C (310K). The OCP (open circuit potential) was determined over 30 minutes, followed by six cycles of CV (cyclic voltammetry) between a potential range of ±500mV vs the

OCP. Stop the measurement and allow it to rest for 30 minutes before repeating the procedure described above. OBS Studio (version 26.0.2) was used to record the microscopic video observations made during the process. Desktop SEM Phenom XL G2 was used to take SEM images (Thermo Fisher Scientific, America). Before SEM, the specimens were cleaned in pure alcohol and blown dry.

2.3 Data collection and analysis

At Ecorr, the exchange current density i_{corr} was calculated from each cyclic I-E curve. In equation (6), the linearized Butler-Volmer equation, the body temperature of 310K, the number of electrons transported per reaction (n=2), the Faraday constant F of 96485 Asmol-1, and the Stern-Geary coefficient of 0.01335 were utilized.

$$I_0 = \frac{RT}{nFR_p} = \frac{Stern-Geary-Coefficient}{R_p} \text{ (A/cm}^2\text{) (6)}$$

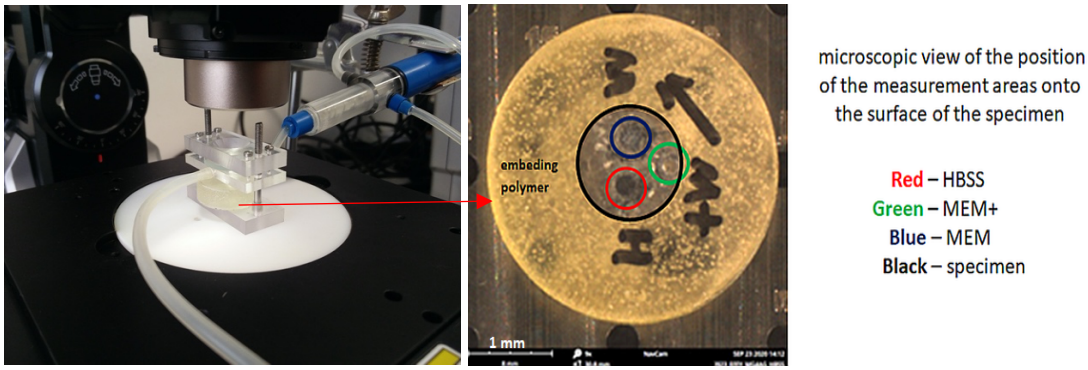

Fig.1: Left: electrochemical flow chamber under the video-microscope (magnification x135); right: the measurement areas on the surface of the specimen for each of the electrolytes [29].

Figure 2 illustrates a particular I vs E cyclic curve with the highlighted data points.

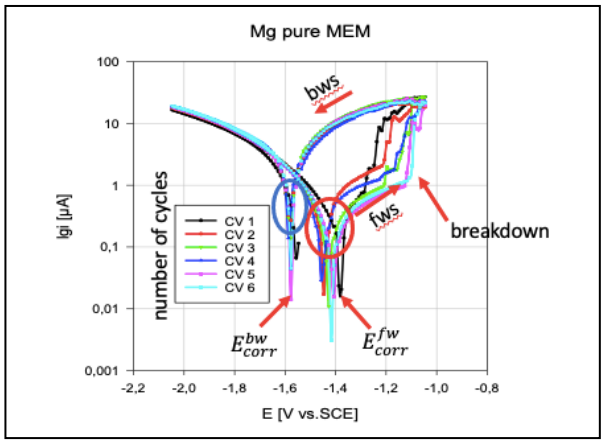

Fig.2: Description of I vs. E curves (The blue circle marks the range of backward scan for assessing I_{corr}, the red circle for the forward scan and the red arrows marked the scan direction and points of interest.[29]

3. Results

3.1 Roughness measurements

The roughness values of the specimens examined are comparable, as indicated by the data in Table 2. Mg2Ag has the maximum degree of roughness, followed by pure Mg specimens, Mg4Ag, and Mg6Ag.

Table 3: Surface roughness of specimens after polishing [29].

materials(µm)	Sa(left)	Sa(right)	Sa(up)	Sa(down)	Sa(middle)	±SD(Sa)
Mg2Ag	1.426	1.688	1.706	1.523	1.747	0.1371
Mg4Ag	1.018	1.233	0.963	1.034	1.187	0.1163
Mg6Ag	1.352	0.932	1.097	0.908	1.138	0.1796
Mg XHP	1.316	1.313	1.337	1.328	1.329	0.0099
Mg Pure	1.341	1.298	1.327	1.305	1.315	0.0172

The images in Figure 3 illustrate the starting states of the MgXAg alloys produced for electrochemical experiments in HBSS, MEM, and MEM+.

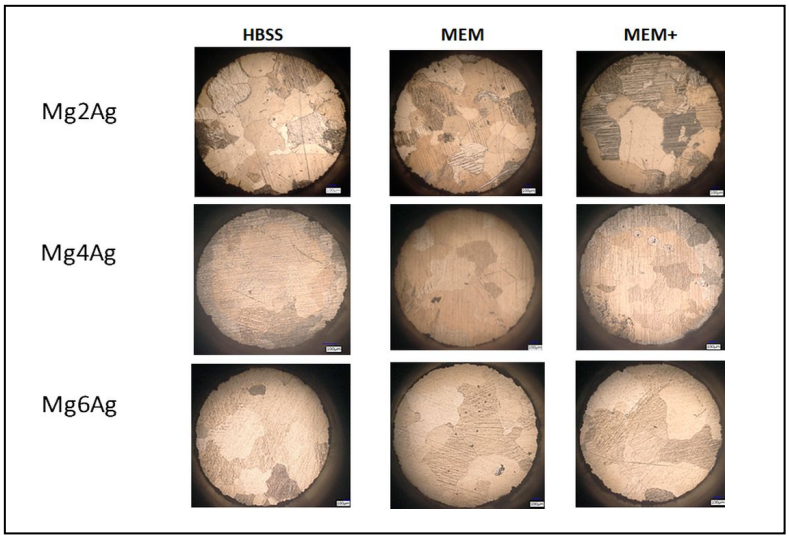

Fig.3: Initial states of MgXAg alloys before the electrochemical measurements in HBSS – MEM and MEM+ [29].

3.2 Electrochemical measurements

As can be observed in Tab. 4, zinc has the highest corrosion rate, whereas Sn has the lowest corrosion rate of all the metals tested. Molybdenum, Zirconium, Nickel and Tin are lower corrosion rate than Mg XHP. The corrosion rate of Iron, Tungsten and Cobalt are between Mg pure and Mg XHP.

Table 4: Comparison of 10 commonly used metals in the MEM electrolyte.（Corrosion rate rating from high to low）

Material	Icorr [A/cm2]	Ecorr [V]	Eocp [V]
Zinc	$4.16 \times 10^{-5} \pm 1.43 \times 10^{-5}$	$1.02 \pm 5.24 \times 10^{-2}$	-1.035
Yttrium	$2.42 \times 10^{-5} \pm 1.21 \times 10^{-5}$	$1.38 \pm 4.08 \times 10^{-3}$	-1.482
Copper	$1.56 \times 10^{-5} \pm 6.67 \times 10^{-6}$	$2.05 \times 10^{-1} \pm 4.12 \times 10^{-2}$	-0.201
Pure Mg	$1.13 \times 10^{-5} \pm 2.16 \times 10^{-6}$	1.38 ± 1.37	-1.463
Iron	$9.83 \times 10^{-6} \pm 3.12 \times 10^{-6}$	$8.04 \times 10^{-1} \pm 2.07 \times 10^{-2}$	-0.218
Tungsten	$7.05 \times 10^{-6} \pm 1.33 \times 10^{-6}$	$5.81 \times 10^{-1} \pm 1.51 \times 10^{-2}$	-0.466
Cobalt	$5.13 \times 10^{-6} \pm 1.74 \times 10^{-6}$	$5.03 \times 10^{-1} \pm 3.55 \times 10^{-2}$	-0.461
XHP Mg	$3.68 \times 10^{-6} \pm 1.12 \times 10^{-6}$	$1.56 \pm 5.48 \times 10^{-3}$	-1.702
Molybdenum	$1.88 \times 10^{-6} \pm 3.69 \times 10^{-7}$	$3.43 \times 10^{-1} \pm 3.63 \times 10^{-2}$	-0.171
Zirconium	$1.07 \times 10^{-6} \pm 1.71 \times 10^{-6}$	$1.71 \times 10^{-1} \pm 7.03 \times 10^{-2}$	-0.395
Nickel	$7.93 \times 10^{-7} \pm 2.22 \times 10^{-7}$	$5.02 \times 10^{-1} \pm 4.85 \times 10^{-2}$	-0.350
Tin	$0.82 \times 10^{-8} \pm 1.61 \times 10^{-8}$	$5.14 \times 10^{-1} \pm 8.16 \times 10^{-3}$	-0.435

Each alloy's OCP values begin at a very cathodic point and progressively rise to a more or less constant value for the course of up to 30 minutes of measurement time, as shown in Fig.4 for the different alloys examined.

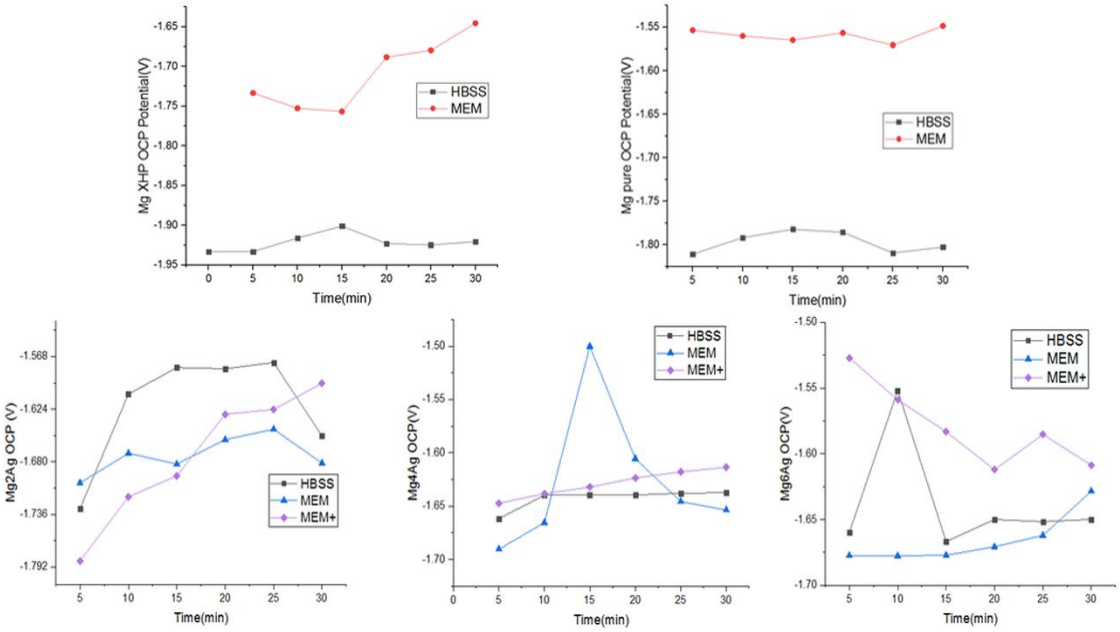

Fig.4: Comparison of the OCP vs. time curves of Mg XHP and Mg pure on the top and MgXAg (from left to right: 2Ag, 4Ag, 6Ag) in MEM , HBSS and MEM+ at 37 ℃ in a flow chamber [29].

Contrary to predictions, no significant variations in the OCP of the MgXAg alloys were discovered. Only in the case of pure and XHP Mg can it be shown that the OCP is moved anodically moved after 30 minutes in MEM compared to HBSS. Table 5 summarizes the final potentials after 30 minutes.

Table 5: Final potential(V) after 30 min OCP in 3 different electrolytes [29].

Mg/Mg alloys	Mg XHP	Mg pure	Mg2Ag	Mg4Ag	Mg6Ag
HBSS	-1.920	-1.802	-1.652	-1.637	-1.649
MEM	-1.645	-1.768	-1.681	-1.653	-1.628
MEM+			-1.596	-1.613	-1.608

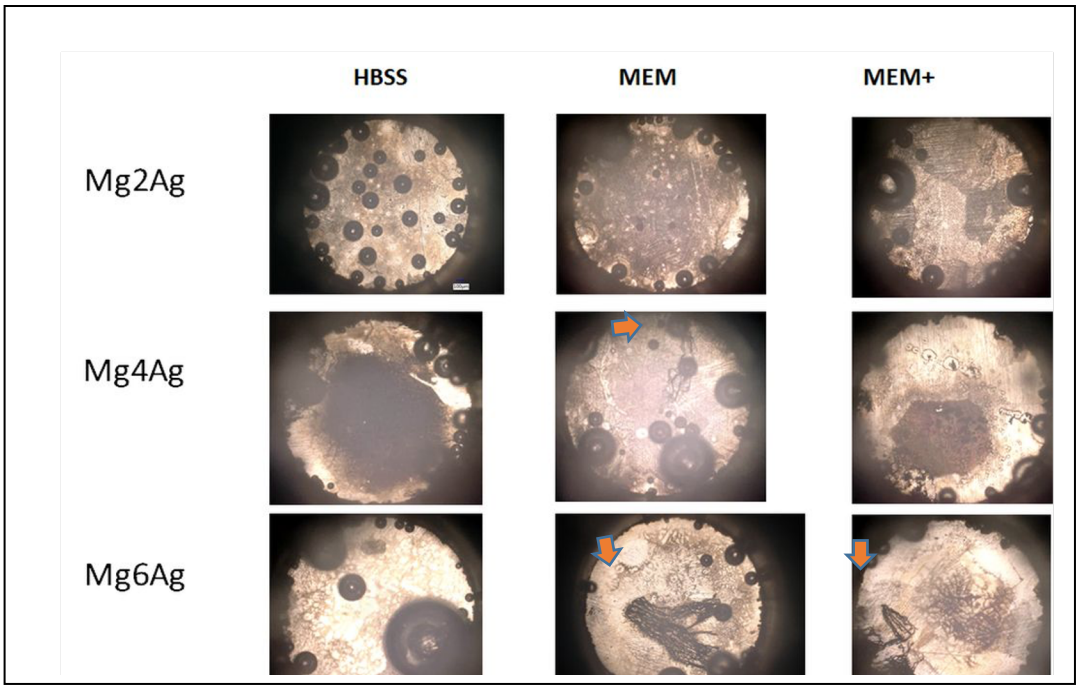

Fig. 5: Situation at the surface of MgXAg alloys after OCP measurements over 30 min in HBSS – MEM and MEM+. Initial degradation is marked by red arrows [29].

Even if the OCP values are hardly different, the pictures demonstrate noticeable changes after 30 minutes, as shown in Fig.5. In HBSS, a difference in the quantity and distribution of HE spots may be noticed compared to the oxide-covered region. All surfaces in MEM exhibit significant oxidation, either by dark staining, as with Mg2Ag, or through pathways of localized "migrating" reactions, as indicated by red arrows on Mg4Ag and Mg6Ag. When $NaHCO_3$ is added to the MEM solution, the early signs of localized oxidation become less visible and are only visible on Mg6Ag.

3.2.1 Cyclic Voltammetry

Cyclic voltammograms exhibit various forms based on the kind of solution and the type of material, pure magnesium or MgXAg alloys. The location of the Ecorr and icorr data varies based on the solution in which they were measured. The pure and XHP Mg behavior under cyclic polarization is entirely different, as seen by the curves in Fig. 6a. In HBSS, neither pure Mg nor MgXHP undergoes breakdown, indicating no extra HE (Hydrogen evolution) occurs during anodic polarization. In MEM, the typical behavior

with rapid hydrogen streams may be observed at some locations near the surface. Typically, very tiny bubbles are formed, appearing like a small stream.

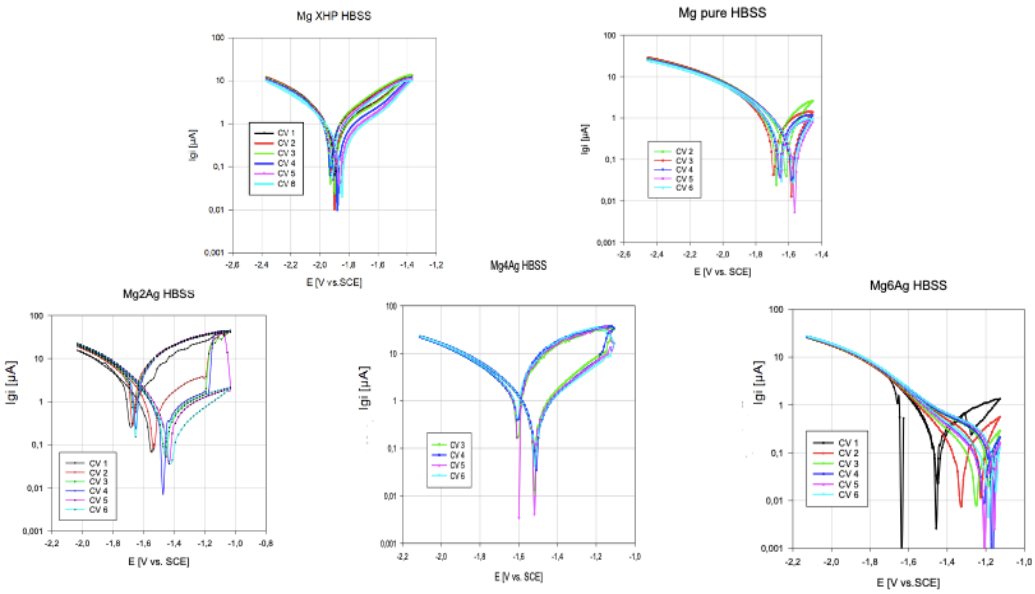

Fig.6a: Comparison of the electrochemical behavior of Mg XHP and Mg pure in HBSS (top) and MgXAg alloys (buttom) at 37°C in a flow chamber [29].

The curves of several MgXAg alloys, polarized in various electrolytes, are shown in Fig 6a–6c. Certain variations in behavior can be noticed depending on the Ag content. Phenomenologically, the behavior of HBSS and MEM+ is comparable to that of MEM, although somewhat different. The CV values obtained for the alloys tested in MEM (Fig. 6b) suggest that magnesium and magnesium–silver alloys exhibit hysteresis. It indicates that the material was subjected to some degree of pitting corrosion during immersion in the electrolytes. It is critical to understand that as silver content increases, the alloys become more susceptible to pitting corrosion. However, as seen in Fig. 6c, this appears to be reduced again when $NaHCO_3$ is added. Mg6Ag exhibits pitting corrosion behavior only during the initial cycle. However, with the passage of time or the number of cycles, the corrosion current decreases.

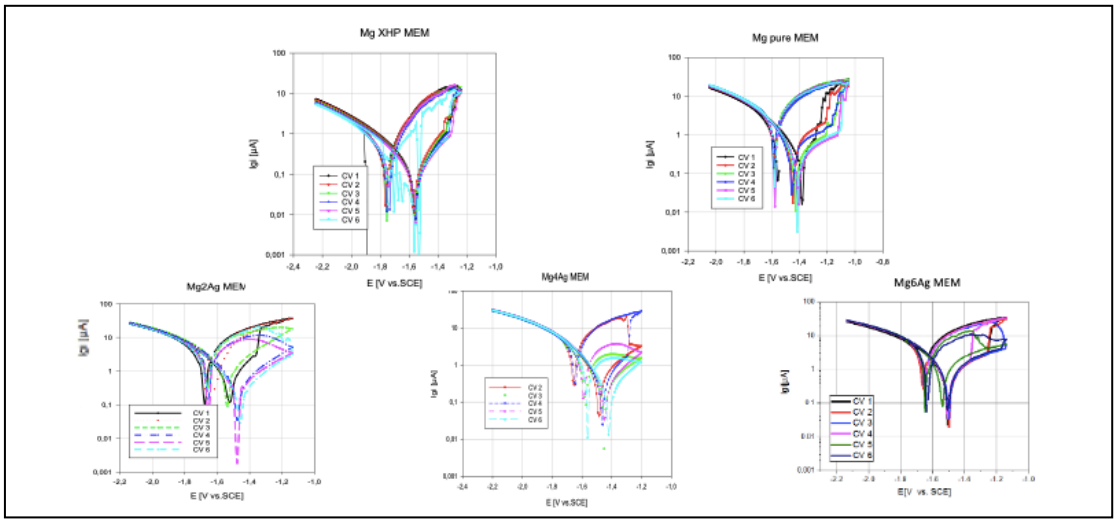

Fig.6b: Comparison of the I vs.E curves of cyclic polarization of Mg XHP and Mg pure in MEM (top) and MgXAg alloys (bottom) at 37 ℃ in a flow chamber [29].

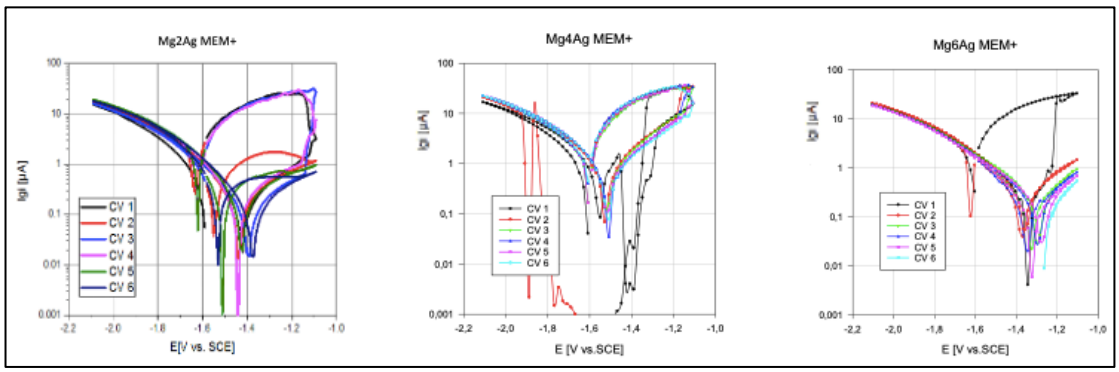

Fig.6c: Comparison of the I vs.E curves of cyclic polarization of MgXAg in MEM+ at 37 ℃ in a flow chamber (the drop down in the curves in case of Mg4Ag is caused by loss of electrical connection by hydrogen gas bubbles adhering to the surface of the specimen) [29].

Table 6 presents the important data for the Ecorr location of the forward and backward scans, as well as the icorr data.

Table 6: The mean values ±SD of E_{corr} and i_{corr} data from 5 cycles forward and backward scan of Mg and MgXAg in HBSS, MEM and MEM+ at 37°C under flow conditions and after 30 mins.

	I [A/cm^2]	E [V vs SCE]	I [A/cm^2]	E [V vs SCE]	I [A/cm^2]	E [V vs SCE]
forward	HBSS		MEM		MEM+	
Mg2Ag	1.24×10^{-4} $\pm4.3\times10^{-6}$	-1.66 ±0.00837	9.79×10^{-5} $\pm1.76\times10^{-5}$	-1.66 ±0.00837	6.24×10^{-5} $\pm3.87\times10^{-5}$	-1.61 ±0.0187
Mg4Ag	1.02×10^{-4} $\pm5.15\times10^{-5}$	-1.54 ±0.0526	1.3×10^{-5} $\pm3.47\times10^{-6}$	-1.45 ±0.0217	5.15×10^{-5} $\pm3.02\times10^{-5}$	-1.61 ±0.0000
Mg6Ag	3.24×10^{-6} $\pm2.63\times10^{-7}$	-1.23 ±0.0559	1.16×10^{-4} $\pm1.92\times10^{-6}$	-1.65 ±0.00837	6.94×10^{-6} $\pm2.11\times10^{-6}$	-1.3 ±0.0349
backward						
Mg2Ag	1.62×10^{-5} $\pm5.17\times10^{-6}$	-1.47 ±0.0367	5.88×10^{-6} $\pm1.09\times10^{-6}$	-1.41 ±0.0311	8.01×10^{-6} $\pm5.04\times10^{-7}$	-1.20 ±0.0336
Mg4Ag	1.25×10^{-4} $\pm1.94\times10^{-5}$	-1.63 ±0.005	6.68×10^{-5} $\pm3.84\times10^{-5}$	-1.6 ±0.0409	2.23×10^{-5} $\pm1.43\times10^{-6}$	-1.52 ±0.00707
Mg6Ag	7.18×10^{-6} $\pm7.78\times10^{-7}$	-1.18 ±0.0311	2.89×10^{-5} $\pm4.04\times10^{-6}$	-1.51 ±0.0164	5.63×10^{-6} $\pm1.19\times10^{-6}$	-1.33 ±0.039

After 30 mins	I [A/cm^2]	E [V vs SCE]	I [A/cm^2]	E [V vs SCE]	I [A/cm^2]	E [V vs SCE]
forward	HBSS		MEM		MEM+	
Mg2Ag	6.49×10^{-6} $\pm1.77\times10^{-6}$	-1.27 ±0.0383	1.11×10^{-5} $\pm2.87\times10^{-6}$	-1.43 ±0.0114	2.09×10^{-5} $\pm3.57\times10^{-5}$	-1.44 ±0.0989
Mg4Ag	1.45×10^{-4} $\pm3.45\times10^{-5}$	-1.6 ±0.0167	2.78×10^{-5} $\pm5.15\times10^{-5}$	-1.42 ±0.117	8.27×10^{-5} $\pm2\times10^{-5}$	-1.59 ±0.00548
Mg6Ag	8.8×10^{-6} $\pm4.09\times10^{-6}$	-1.37 ±0.0286	9.99×10^{-5} $\pm2.96\times10^{-5}$	-1.55 ±0.0513	4.78×10^{-6} $\pm5.8\times10^{-7}$	-1.26 ±0.0249
backward						
Mg2Ag	8.01×10^{-6} $\pm5.04\times10^{-7}$	-1.20 ±0.0336	3.9×10^{-5} $\pm3.96\times10^{-5}$	-1.53 ±0.055	4.79×10^{-6} $\pm1.38\times10^{-6}$	-1.41 ±0.0259
Mg4Ag	4.5×10^{-5} $\pm3.19\times10^{-5}$	-1.41 ±0.0167	5.52×10^{-6} $\pm3.11\times10^{-6}$	-1.1 ±0.617	2.48×10^{-5} $\pm5.82\times10^{-6}$	-1.5 ±0.0249
Mg6Ag	8.93×10^{-6} $\pm4.03\times10^{-6}$	-1.33 ±0.0716	8.11×10^{-5} $\pm2.62\times10^{-5}$	-1.51 ±0.051	4.73×10^{-6} $\pm4.24\times10^{-7}$	-1.23 ±0.0205

The data collected during the electrochemical experiment, which lasted about two hours, could not be used to derive an exact rule. However, it may be used to derive a general law. The corrosion rate of the second group is lower than the corrosion rate of the first group when measured in terms of time. Comparing the MEM+ group to the MEM group, it is comparatively low in terms of corrosion rate. As the silver content of the alloy rises in the same electrolyte simultaneously, the alloy exhibits an increase in corrosion rate in MEM while exhibiting a reduction in corrosion rate in HBSS and MEM+. However, it is necessary to monitor the specificity of Mg4Ag over a more extended period.

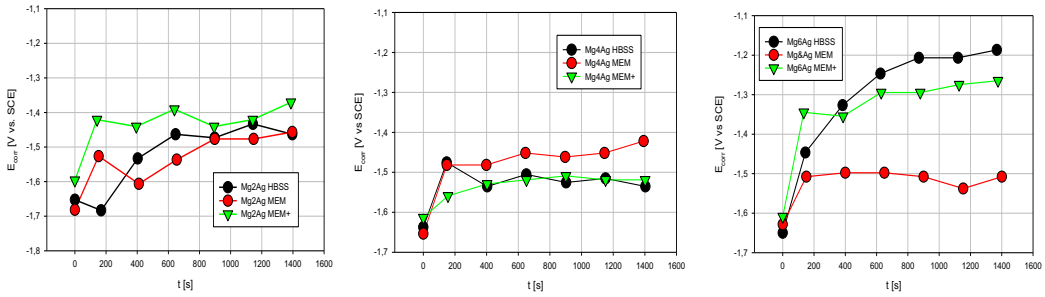

Fig.7: Changes of E_{corr} of the forward scan with time for MgXAg alloys in 3 different electrolytes at 37°C und flowing conditions [29]. The evolution of Ecorr over time, which is also related to the number of cycles.

Ecorr exhibits an anodic change with time in all of these situations. The apparent anodic shift of Ecorr for Mg6Ag in electrolytes containing $NaHCO_3$ is unexpected. Additionally, the results demonstrate that when Ecorr potentials are anodically moved, the values of icorr are substantially lower than when they are more cathodically situated, as seen in Fig. 8a - 8c.

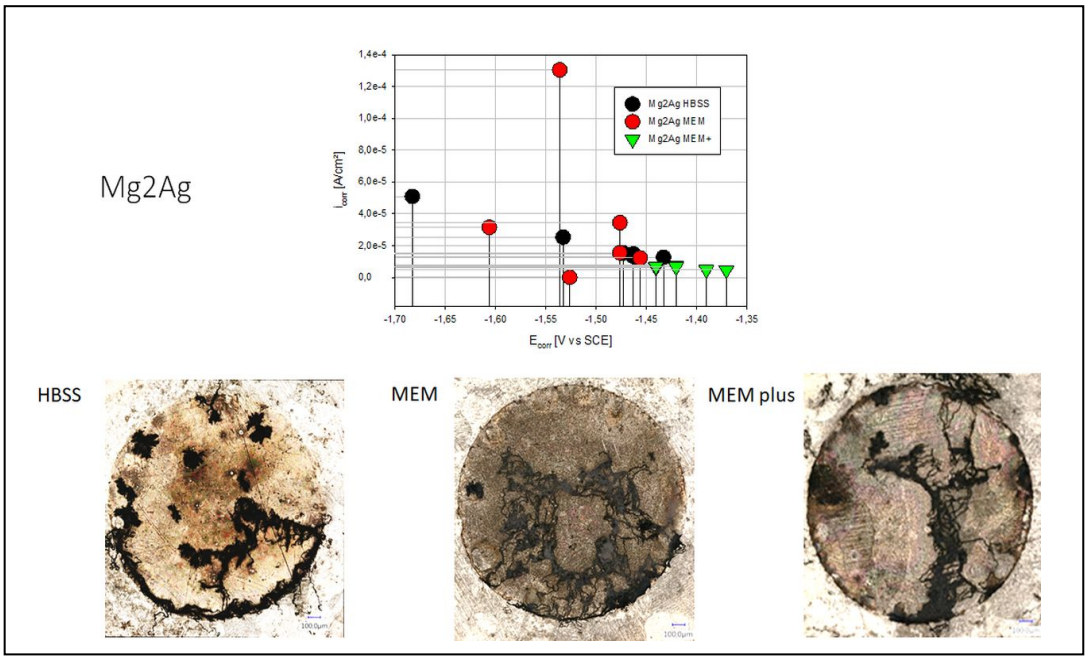

Fig.8a: Comparison of i_{corr} vs. E_{corr} data from cyclic polarization (top) of Mg2Ag alloy in HBSS, MEM and MEM+ together with the situation at the surface after the electrochemical measurements [29].

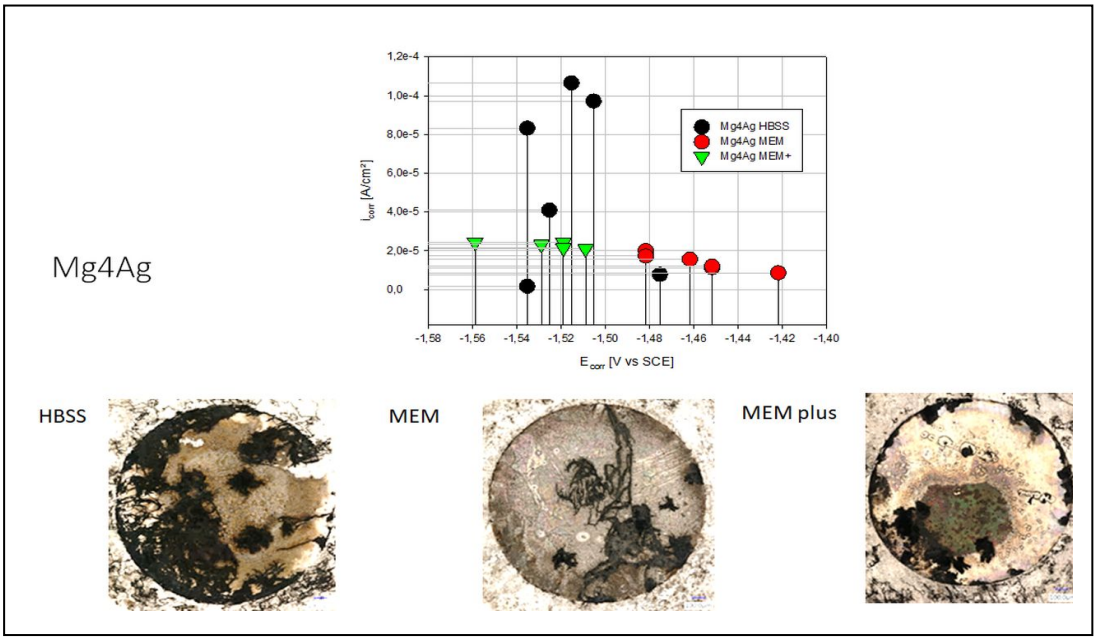

Fig.8b: Comparison of i_{corr} vs. E_{corr} data from cyclic polarization (top) of Mg4Ag alloy in HBSS, MEM and MEM+ together with the situation at the surface after the electrochemical measurements [29].

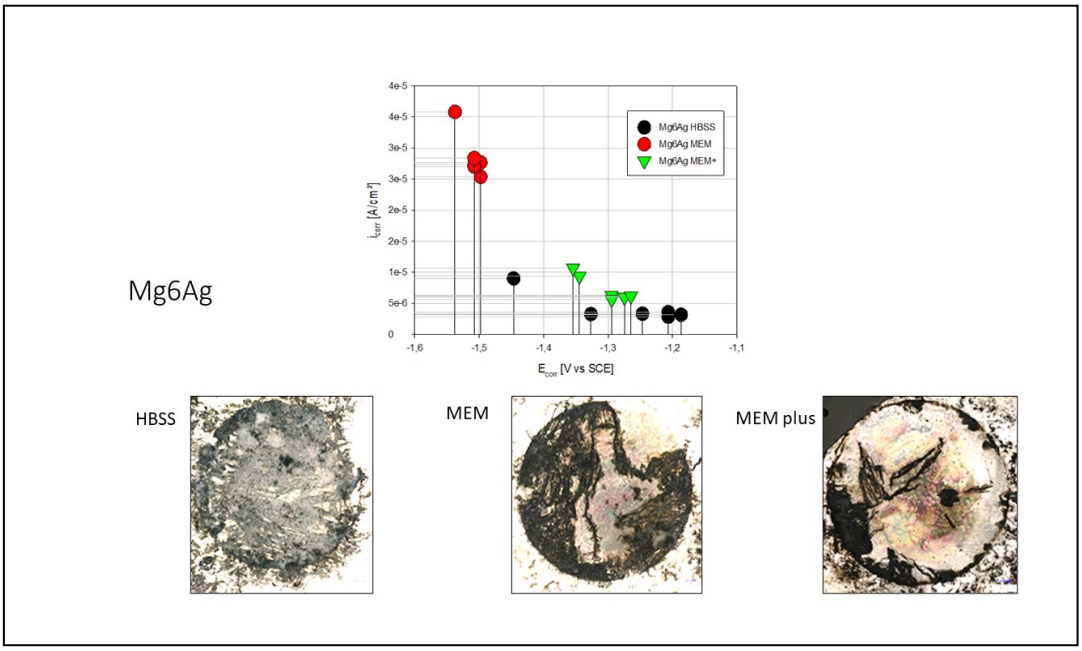

Fig.8c: Comparison of i_{corr} vs. E_{corr} data from cyclic polarization (top) of Mg6Ag alloy in HBSS, MEM and MEM+ together with the situation at the surface after the electrochemical measurements. The video microscopic view before (left) Mag: x=150 and after (right) Mag.: x=300; 2.5 hours after the end of the experiment[29].

The surfaces following electrochemical polarization are shown in Figures 8a–8c.

Except for Mg6Ag in HBSS, visible alterations on the surfaces may be observed following treatment. Localized "moving" oxidation processes are seen as black, meandering lines. Pitting is visible in the instance of Mg4Ag in MEM plus, which is characteristic of static electrolytes. Mg6Ag in HBSS astonishes with a nearly uniform covering of the surface by an oxide layer devoid of visible deterioration spots.

3.3 Scanning electron microscopy (SEM)

MgXAg specimens after 130 minutes of electrochemical testing in three different electrolytes are seen in SEM images (Fig.9). The major corrosion products observed in pits and fractures are magnesium oxide (MgO) and magnesium hydroxide ($Mg(OH)_2$) [26]. Electrochemical research indicated that all three alloys had a non-circular concavity pattern with a depressed surface irregularly spaced. Mg2Ag corroded evenly and pitted, but Mg6Ag corroded gently and uniformly compared to the other two alloys in the same electrolytes. When $NaHCO_3$ is added to the same alloyed MEM electrolyte, visibly larger pits form.

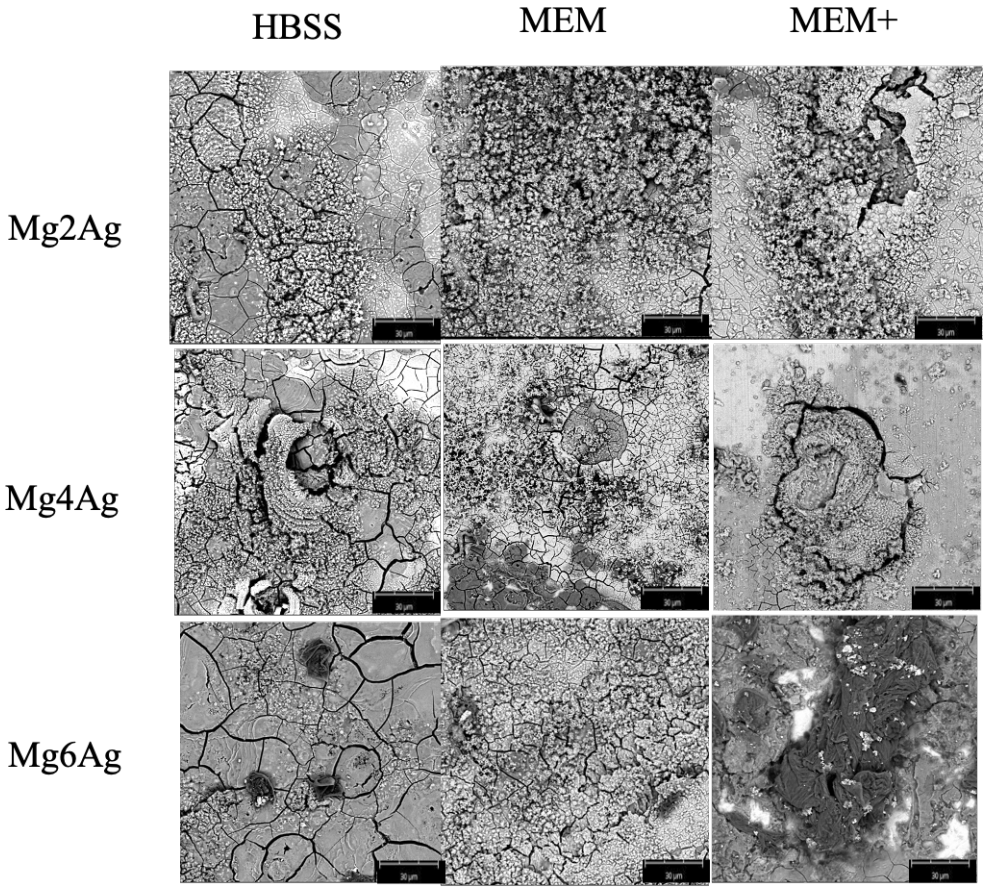

Fig.9: Three MgXAg alloys showing special surface structure, SEM after 200mins electrochemistry experiment [29].

4. Discussion

Mg-based biometals (BMs) degrade at a quick speed in body fluid according to our research. With such a fast degradation rate, it would be possible for it to lose mechanical integrity in a short amount of time, which would restrict its use as an implant material. Magnesium alloy corrosion is mostly galvanic couple corrosion, corrosion of the second phase or impurity phase as a cathode phase[32]. For Fe, Cu, Ni, etc. present in the interior of magnesium alloy, and the substrate alloy constitutes a corrosion microcell of Mg Alloy. As for Zn, Y, etc., to a certain extent, because of its high hydrogen overpotential, it is expected to improve the corrosion resistance of magnesium alloys to a certain extent.

The current exchange densities of (i_{corr} or i_0) indicate the intrinsic electron transfer rates between an analyte and an electrode [33], [34]. These rates give information on the composition and interactions of the analyte and electrode. Through this test, we have a comprehensive understanding of the degradation process of magnesium and its alloys, and it is crucial to quantify the excess of HE on the magnesium surface [35].

According to our inquiry and aim, we expected to uncover a consistent relationship between electrochemical behavior, precisely when measuring the current exchange density, which measures the rate of degradation in an in-vitro environment, and the electrolyte composition. Second, we want to investigate the influence of visible changes on MgXAg alloys during open circuit degradation and electrochemical polarization [16], [19].

As demonstrated by the results given here, there is a difference in Mg XHP and Mg pure electrochemical behavior depending on the in-vitro solutions utilized by HBSS and MEM. A third electrolyte, MEM+, was employed to replicate the CO_2 buffer activity in MEM for the MgXAg alloys tests.

The results collected in this experiment showed no apparent systematic explanation for the differences in the electrochemical performance between the various MgXAg alloys. Comparing optical recordings taken before and after polarization (using cyclic voltammetry) shows that a surface already showing signs of corrosion will be attacked more severely. However, polarization may significantly impact a surface that was only slightly oxidized to begin with[36], [37].

This can be attributed to various factors depending on the alloy composition and structure, including grain size position and orientation and chemical activity [18].

No particular areas could be observed that might be attributed to hydrogen evolution or the oxidation and precipitation of more minor soluble compounds near the surface, based on our observations. Each examined surface had its distinct structure, as seen in Fig.8a-c after the treatments.

When exposed to an aqueous solution (such as MEM or HBSS solution), corrosion occurs on the border of the growing patch, causing the corrosion product to precipitate in the region. Magnesium corrosion products have been shown to have enhanced catalytic activity against human epidermal growth factor receptors [14]–[16].

By evaluating both the forward and backward scans for the electrochemical activity of the various MgXAg alloys, it is possible to observe a minor correlation between the Ag content and the anodic shift of Ecorr at the peak of icorr. In Mg6Ag, the electrolytes containing CO_2, HBSS and MEM+, exhibit the same activity as the CO_2-free electrolyte (MEM). However, as seen in Fig. 10a and 10b, it is not visible in the case of Mg2Ag and Mg4Ag.

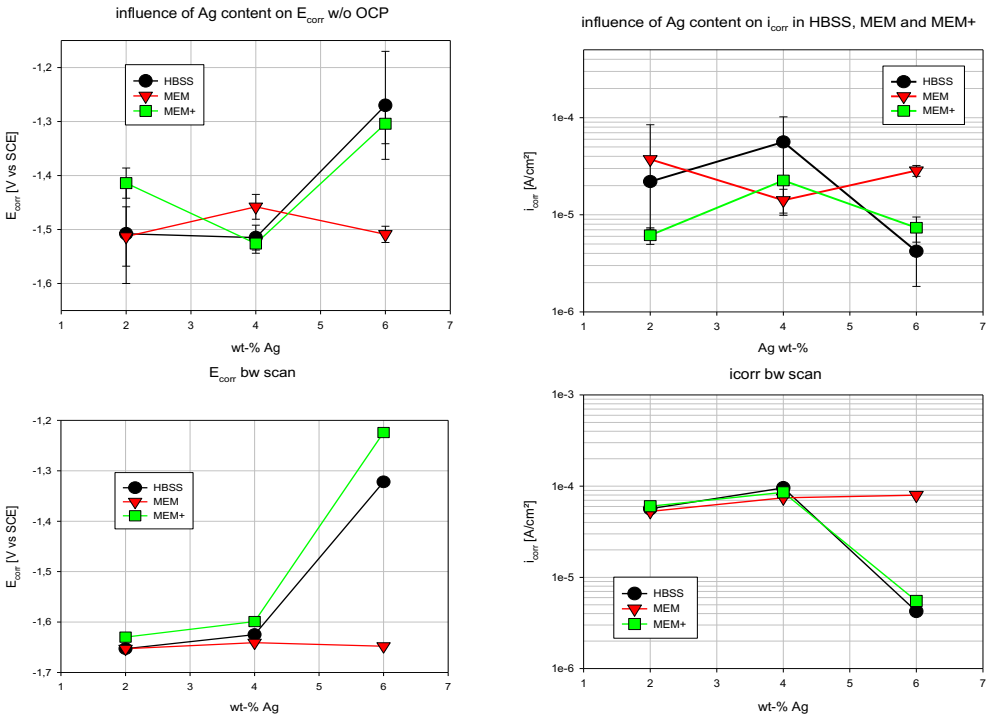

Fig.10: Assessment of forwarding (top) and backward (bottom) scan for three different MgXAg alloys in 3 different electrolytes [29].

As seen in the SEM pictures in Fig.9, pitting corrosion was identified as the most effective form of deterioration at the end. The inhomogeneity of the metal surface is a significant

cause of pitting corrosion [38]. It is crucial to understand why and when the concentration of chloride ions in the solution increases, and the breakdown process accelerates [20]. These circumstances are confusing for electrochemical analysis of magnesium and magnesium alloy degradation [39]–[41]. The decrease in active reaction area and the connection between anodic and cathodic reaction pathways complicate degradation prediction[37]. The video-optical setup provides additional information about the effect of the electrolyte composition on the degradation behavior of MgXAg alloys, as the images changed throughout the investigation, namely the changing positions of the oxidation, which impose, as mentioned earlier, as meandering black lines, and additionally, specific sites for hydrogen production were identified in the vicinity of which no apparent changes in the surface appearance was observed.

This complicates obtaining an accurate picture of magnesium and magnesium alloys deterioration. The apparent changes on the surfaces, which were interpreted in some instances as a significant deterioration and alteration of the surface, were not well represented in the electrochemical data, as described in Fig.11.

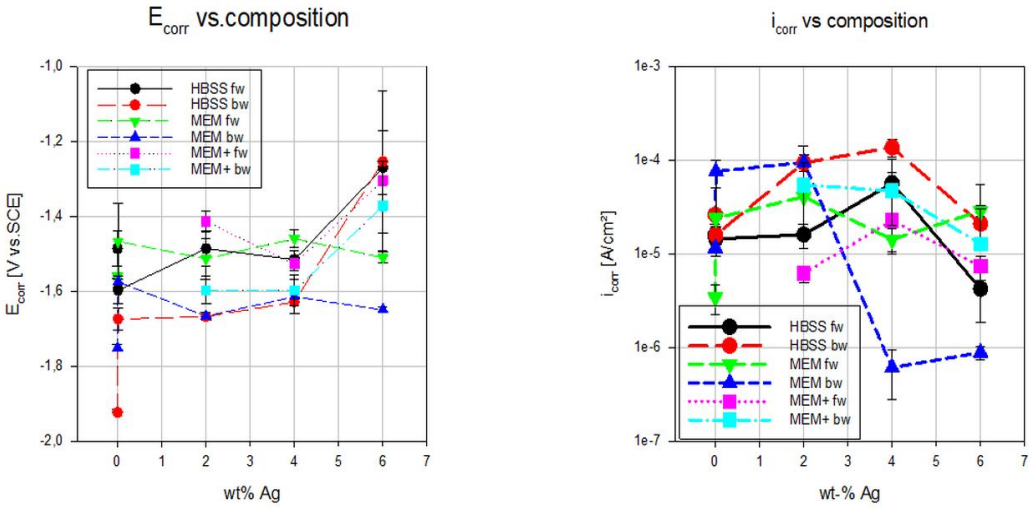

Fig.11: Influence of the Ag-content on Ecorr (left) and icorr (right). Comparison of the data from cyclic voltammetry divided into forwarding and backward scan [29].

Only a trend of deterioration can be determined due to the galvanically coupled response on the surface. Additional studies are required to determine the critical influence or location(s) of surface modifications linked with the observed electrochemical activity.

5. Conclusion

The varying rates of corrosion from one phase to another influenced the mechanism of pitting corrosion. The corrosion potential of Mg–Ag metallic compounds was moved in anodic direction by adding silver content. The composition of the alloy as well as the composition of the electrolyte have a significant influence on the electrochemical performance of the investigated alloys. Most interestingly, we discovered that the silver content is a critical element in pitting corrosion protection of magnesium alloys while keeping the overall corrosion rate under control. It is also vital to pay more attention to the concept of protein evoked effects during magnesium corrosion, as it undoubtedly plays an important role in reducing both homogeneous and pitting corrosion of magnesium materials used in the body. Dependent on this performance, biodegradable implants containing MgXAg binary alloys would have a multifunctional use. In the next step the observation period can be extended, or the pH changed to monitor changes in the magnesium corrosion site. It is also our aim to track the factors influencing the trend of pitting corrosion during the reaction.

6. Summary

Apparent surface activity correlates to high electrochemical activity, although the relationship between composition and activity is not consistently established. The fluctuating rates of corrosion influenced the pitting corrosion process throughout stages of the corrosion process. The corrosion potential of magnesium–silver metallic complexes was changed from the cathodic to the anodic direction by increasing the silver concentration. The composition of the alloy and the composition of the electrolyte have a significant impact on the electrochemical performance of the alloys under investigation. Most intriguingly, we discovered that silver in magnesium alloys plays a critical role in preserving them from pitting corrosion while also reducing the overall rate of corrosion. Also important is paying greater attention to the notion of protein-evoked effects during magnesium corrosion. This concept unquestionably plays a significant role in reducing both homogeneous and pitting corrosion of magnesium materials used in the body. MgXAg binary alloys, which are used to make biodegradable implants, offer a wide range of potential uses, depending on their performance. If the magnesium corrosion site changes are seen, the observation period may be extended, or the pH may be changed in

the next step, if necessary. In addition, we would like to keep track of the factors that impact the pitting corrosion trend throughout the reaction.

7. References

[1] G. Y. Liu, J. Hu, Z. K. Ding, and C. Wang, "Bioactive calcium phosphate coating formed on micro-arc oxidized magnesium by chemical deposition," *Appl. Surf. Sci.*, vol. 257, no. 6, pp. 2051–2057, 2011, doi: 10.1016/j.apsusc.2010.09.050.

[2] C. Janning, E. Willbold, C. Vogt, J. Nellesen, A. Meyer-Lindenberg, H. Windhagen, F. Thorey and F. Witte, "Magnesium hydroxide temporarily enhancing osteoblast activity and decreasing the osteoclast number in peri-implant bone remodelling," *Acta Biomater.*, vol. 6, no. 5, pp. 1861–1868, 2010, doi: 10.1016/j.actbio.2009.12.037.

[3] F. Witte, "Acta Biomaterialia The history of biodegradable magnesium implants : A review q," *Acta Biomater.*, vol. 6, no. 5, pp. 1680–1692, 2010, doi: 10.1016/j.actbio.2010.02.028.

[4] H. S. Brar, M. O. Platt, M. Sarntinoranont, P. I. Martin, and M. V. Manuel "Magnesium as a biodegradable and bioabsorbable material for medical implants," *Jom*, vol. 61, no. 9, pp. 31–34, 2009, doi: 10.1007/s11837-009-0129-0.

[5] B. G. Song and A. Atrens, "Understanding Magnesium Corrosion A Framework for Improved Alloy Performance **," no. 12, pp. 837–858, 2003, doi: 10.1002/adem.200310405.

[6] H. Wu, C Zhang, T. Lou, B. Chen, R. Yi, W. Wang, R. Zhang, M. Zuo, H. Xu, P. Han, S. Zhang, J. Ni and X. Zhang, "Crevice corrosion – A newly observed mechanism of degradation in biomedical magnesium," *Acta Biomater.*, vol. 98, pp. 152–159, 2019, doi: 10.1016/j.actbio.2019.06.013.

[7] Y. Xin, K. Huo, H. Tao, G. Tang, and P. K. Chu, "Influence of aggressive ions on the degradation behavior of biomedical magnesium alloy in physiological environment," *Acta Biomater.*, vol. 4, no. 6, pp. 2008–2015, 2008, doi: 10.1016/j.actbio.2008.05.014.

[8] Z. Shi, J. X. Jia, and A. Atrens, "Galvanostatic anodic polarisation curves and galvanic corrosion of high purity Mg in 3 . 5 % NaCl saturated with Mg (OH) 2," *Corros. Sci.*, vol. 60, pp. 296–308, 2012, doi: 10.1016/j.corsci.2011.12.002.

[9] B. Kwakye-Awuah, C. Williams, M. A. Kenward, and I. Radecka, "Antimicrobial action and efficiency of silver-loaded zeolite X," *J. Appl. Microbiol.*, vol. 104, no. 5, pp. 1516–1524, 2008, doi: 10.1111/j.1365-2672.2007.03673.x.

[10] S. Silver, L. T. Phung, and G. Silver, “Silver as biocides in burn and wound dressings and bacterial resistance to silver compounds,” *J. Ind. Microbiol. Biotechnol.*, vol. 33, no. 7, pp. 627–634, 2006, doi: 10.1007/s10295-006-0139-7.

[11] A. B. G. Lansdown, “Silver in Health Care: Antimicrobial Effects and Safety in Use Interactions between Skin and Biofunctional Metals,” *Curr. Probl. Dermatol.*, vol. 33, pp. 17–34, 2006.

[12] X. Gu, Y. Zheng, Y. Cheng, S. Zhong, and T. Xi, “Biomaterials In vitro corrosion and biocompatibility of binary magnesium alloys,” *Biomaterials*, vol. 30, no. 4, pp. 484–498, 2009, doi: 10.1016/j.biomaterials.2008.10.021.

[13] Y. H. Kim, W. S. Chung, H. H. Chun, I. Lee, Y. H. Kim, D. H. Kim and H. Park “The effect of ball milling on the pH of Mg-based metals, oxides and Zn in aqueous media,” *Met. Mater. Int.*, vol. 16, no. 2, pp. 253–258, 2010, doi: 10.1007/s12540-010-0414-z.

[14] G. Song, “Control of biodegradation of biocompatable magnesium alloys,” vol. 49, pp. 1696–1701, 2007, doi: 10.1016/j.corsci.2007.01.001.

[15] P. Rosemann, J. Schmidt, and A. Heyn, “Short and long term degradation behaviour of Mg-1Ca magnesium alloys and protective coatings based on plasma-chemical oxidation and biodegradable polymer coating in synthetic body fluid,” *Mater. Corros.*, vol. 64, no. 8, pp. 714–722, 2013, doi: 10.1002/maco.201206590.

[16] N. Ahmad, F. Feyerabend, B. Mihailova, S. Heidrich, U. Bismayer, and R. Willumeit-römer, “Magnesium degradation in fl uenced by buffering salts in concentrations typical of in vitro and in vivo models,” *Mater. Sci. Eng. C*, vol. 58, pp. 817–825, 2016, doi: 10.1016/j.msec.2015.09.067.

[17] D. Tie, F. Feyerabend, W. Müller, R. Schade, K. Liefeith, and K. U. Kainer, “ANTIBACTERIAL BIODEGRADABLE Mg-Ag ALLOYS,” vol. 25, pp. 284–298, 2013, doi: 10.22203/eCM.v025a20.

[18] J. Gonzalez, R. Q. Hou, E. P. S. Nidadavolu, R. Willumeit-Römer, and F. Feyerabend, “Magnesium degradation under physiological conditions – Best practice,” *Bioact. Mater.*, vol. 3, no. 2, pp. 174–185, 2018, doi: 10.1016/j.bioactmat.2018.01.003.

[19] S. Virtanen, I. Milošev, E. Gomez-Barrena, R. Trebše, J. Salo, and Y. T. Konttinen, “Special modes of corrosion under physiological and simulated physiological

conditions," *Acta Biomater.*, vol. 4, no. 3, pp. 468–476, 2008, doi: 10.1016/j.actbio.2007.12.003.

[20] A. Witecka, A. Bogucka, A. Yamamoto, K. Máthis,T Krajňák, J. Jaroszewicz and W. Święszkowski "In vitro degradation of ZM21 magnesium alloy in simulated body fluids," *Mater. Sci. Eng. C*, vol. 65, pp. 59–69, 2016, doi: 10.1016/j.msec.2016.04.019.

[21] C. Taltavull, Z. Shi, B. Torres, J. Rams, and A. Atrens, "Influence of the chloride ion concentration on the corrosion of high-purity Mg , ZE41 and AZ91 in buffered Hank ' s solution," pp. 329–345, 2014, doi: 10.1007/s10856-013-5087-y.

[22] M. Sumita, T. Hanawa, and I. Ohnishi, "Failure Processes in Biometallic Materials," *Compr. Struct. Integr.*, pp. 131–167, 2003.

[23] D. Hong, S. H. Zaky, R. Chong, L. Lukashova, E. Beniash, K. Verdelis, F.Witte and C. Sfeir "Controlling magnesium corrosion and degradation-regulating mineralization using matrix GLA protein," *Acta Biomater.*, vol. 98, pp. 142–151, 2019, doi: 10.1016/j.actbio.2019.05.048.

[24] Y. Li, Q. Pan, J. Xu, X. He, H. A. Li, D. A.Oldridge, G. Li and L. Qin, "Overview of methods for enhancing bone regeneration in distraction osteogenesis: Potential roles of biometals," *J. Orthop. Transl.*, vol. 27, pp. 110–118, 2021, doi: https://doi.org/10.1016/j.jot.2020.11.008.

[25] K. D. Fasae, K. D.Fasae, A. O. Abolaji, T. R. Faloye, A. Y. Odunsi, B. O.Oyetayo, J. I. Enya, J. A. Rotimi, R. O. Akinyemi, A. J.Whitworth, M. Aschnerg "Metallobiology and therapeutic chelation of biometals (copper, zinc and iron) in Alzheimer's disease: Limitations, and current and future perspectives," *J. Trace Elem. Med. Biol.*, vol. 67, p. 126779, 2021, doi: https://doi.org/10.1016/j.jtemb.2021.126779.

[26] H. Dong, F. Lin, A. R. Boccaccini, and S. Virtanen, "Corrosion behavior of biodegradable metals in two different simulated physiological solutions: Comparison of Mg, Zn and Fe," *Corros. Sci.*, vol. 182, p. 109278, 2021, doi: https://doi.org/10.1016/j.corsci.2021.109278.

[27] D. Xia, F. Yang, Y. Zheng, Y. Liu, and Y. Zhou, "Research status of biodegradable metals designed for oral and maxillofacial applications: A review," *Bioact. Mater.*, vol. 6, no. 11, pp. 4186–4208, 2021, doi: https://doi.org/10.1016/j.bioactmat.2021.01.011.

[28] G. Song, *Corrosion electrochemistry of magnesium (Mg) and its alloys*. Woodhead Publishing Limited, 2011.

[29] Y. Zhang, T. Zimmermann, W.-D. Mueller, F. Witte, F. Beuer, and A. Schwitalla, "Exploring the degradation behavior of MgXAg alloys by in vitro electrochemical methods," *Bioact. Mater.*, 2021, doi: 10.1016/j.bioactmat.2021.05.044.

[30] Y. Yang, F. Scenini, and M. Curioni, "Electrochimica Acta A study on magnesium corrosion by real-time imaging and electrochemical methods : relationship between local processes and hydrogen evolution," *Electrochim. Acta*, vol. 198, pp. 174–184, 2016, doi: 10.1016/j.electacta.2016.03.043.

[31] T. Zimmermann, N. Hort, Y. Zhang, W. D. Müller, and A. Schwitalla, "The video microscopy-linked electrochemical cell: An innovative method to improve electrochemical investigations of biodegradable metals," *Materials (Basel).*, vol. 14, no. 7, 2021, doi: 10.3390/ma14071601.

[32] S. V Dorozhkin, "7 - Surface modification of magnesium and its biodegradable alloys by calcium orthophosphate coatings to improve corrosion resistance and biocompatibility," in *Woodhead Publishing Series in Biomaterials*, T. S. N. S. Narayanan, I.-S. Park, and M.-H. B. T.-S. M. of M. and its A. for B. A. Lee, Eds. Woodhead Publishing, 2015, pp. 151–191.

[33] H. Hornberger, F. Witte, N. Hort, and W. Mueller, "Effect of fetal calf serum on the corrosion behaviour of magnesium alloys," *Mater. Sci. Eng. B*, vol. 176, no. 20, pp. 1746–1755, 2011, doi: 10.1016/j.mseb.2011.07.018.

[34] R. G. Kelly, J. R. Scully, D. W. Shoesmith, and R. G. Buchheit, *Electrochemical Techniques in Corrosion Science and Engineering*. .

[35] D. Tie, F. Feyerabend, N. Hort, D. Hoeche, K. U. Kainer, R. Willumeit and W. D. Mueller, "In vitro mechanical and corrosion properties of biodegradable Mg – Ag alloys," no. 6, pp. 569–576, 2014, doi: 10.1002/maco.201206903.

[36] S. Fajardo and G. S. Frankel, "Effect of impurities on the enhanced catalytic activity for hydrogen evolution in high purity magnesium," *Electrochim. Acta*, vol. 165, pp. 255–267, 2015, doi: 10.1016/j.electacta.2015.03.021.

[37] N. Birbilis, G. Williams, K. Gusieva, A. Samaniego, M. A. Gibson, and H. N. Mcmurray, "Electrochemistry Communications Poisoning the corrosion of magnesium," *Electrochem. commun.*, vol. 34, pp. 295–298, 2013, doi: 10.1016/j.elecom.2013.07.021.

[38] M. Curioni, “Electrochimica Acta The behaviour of magnesium during free corrosion and potentiodynamic polarization investigated by real-time hydrogen measurement and optical imaging,” *Electrochim. Acta*, vol. 120, pp. 284–292, 2014, doi: 10.1016/j.electacta.2013.12.109.

[39] Y. Gao, L. Wang, L. Li, X. Gu, K. Zhang, J. Xia and Yubo Fan “Effect of stress on corrosion of high-purity magnesium in vitro and in vivo,” *Acta Biomater.*, vol. 83, pp. 477–486, 2019, doi: 10.1016/j.actbio.2018.11.019.

[40] N. T. Kirkland, J. Lespagnol, N. Birbilis, and M. P. Staiger, “A survey of bio-corrosion rates of magnesium alloys,” *Corros. Sci.*, vol. 52, no. 2, pp. 287–291, 2010, doi: 10.1016/j.corsci.2009.09.033.

[41] F. Witte, N. Hort, F. Feyerabend, and C. Vogt, “Magnesium (Mg) corrosion: A challenging concept for degradable implants,” *Corros. Magnes. Alloy.*, pp. 403–425, 2011, doi: 10.1533/9780857091413.3.403.

Statutory Declaration

"I, Yuqiuhan Zhang, by personally signing this document in lieu of an oath, hereby affirm that I prepared the submitted dissertation on the topic **"Assessing the degradation behavior of magnesium alloys using electrochemical methods / Beurteilung des Abbauverhaltens von Magnesiumlegierungen mit elektrochemischen Methoden"**, independently and without the support of third parties, and that I used no other sources and aids than those stated.

All parts which are based on the publications or presentations of other authors, either in letter or in spirit, are specified as such in accordance with the citing guidelines. The sections on methodology (in particular regarding practical work, laboratory regulations, statistical processing) and results (in particular regarding figures, charts and tables) are exclusively my responsibility.

[In the case of having conducted your doctoral research project completely or in part within a working group:] Furthermore, I declare that I have correctly marked all of the data, the analyses, and the conclusions generated from data obtained in collaboration with other persons, and that I have correctly marked my own contribution and the contributions of other persons (cf. declaration of contribution). I have correctly marked all texts or parts of texts that were generated in collaboration with other persons.

My contributions to any publications to this dissertation correspond to those stated in the below joint declaration made together with the supervisor. All publications created within the scope of the dissertation comply with the guidelines of the ICMJE (International Committee of Medical Journal Editors; www.icmje.org) on authorship. In addition, I declare that I shall comply with the regulations of Charité – Universitätsmedizin Berlin on ensuring good scientific practice.

I declare that I have not yet submitted this dissertation in identical or similar form to another Faculty.

The significance of this statutory declaration and the consequences of a false statutory declaration under criminal law (Sections 156, 161 of the German Criminal Code) are known to me."

Date Signatur

Declaration of your own contribution to the publications

Yuqiuhan Zhang contributed the following to the below listed publication:

Publication:
Yuqiuhan Zhang, Tycho Zimmermann, Wolf-Dieter Mueller, Frank Witte, Florian Beuer, Andreas Schwitalla. Exploring the degradation behavior of MgXAg alloys by in vitro electrochemical methods. Bioactive Materials, 2021.

Contribution:
Participated in project conception; Designed and tested the protocol; Participated in electrochemical flow chamber design, improvement and fabrication; Performed the pre-experiment.
Prepared experimental materials and performed the formal experiments, including specimen electrolyte preparation, polishing and etching, roughness measurement, grain size analysis, electrochemical measurement, set up the electrolyte circulation with body temperature in vitro, SEM.

Data collection, data statistically analysis and surface reaction visualization. Figures and tables were generated on the basis of my results of experiments and statistical evaluation. Tables 1, 2, 3, 4, 5, 6

and figure 1, 2, 3, 4, 5, 6a-c, 9(the details in the table below) were created on the basis of my statistical evaluation; Drafted and revised the manuscript.

Figures	1	*left: electrochemical flow chamber under the video-microscope (magnification x135) right: the measurement areas on the surface of the specimen for each of the electrolytes.*
	2	*Description of I vs. E curves*
	3	*Initial states of MgXAg alloys before the electrochemical measurements in HBSS – MEM and MEM+*
	4	*Comparison of the OCP vs. time curves of Mg XHP and Mg pure on the top and MgXAg (from left to right: 2Ag, 4Ag, 6Ag) in MEM , HBSS and MEM+ at 37°C in a flow chamber*
	5	*Situation at the surface of MgXAg alloys after OCP measurements over 30 min in HBSS – MEM and MEM+. Initial degradation is marked by red arrows*
	6a	*Comparison of the electrochemical behavior of Mg XHP and Mg pure in HBSS (top) and MgXAg alloys (buttom) at 37°C in a flow chamber*
	6b	*Comparison of the I vs.E curves of cyclic polarization of Mg XHP and Mg pure in MEM (top) and MgXAg alloys (bottom) at 37°C in a flow chamber*
	6c	*Comparison of the I vs.E curves of cyclic polarization of MgXAg in MEM+ at 37°C in a flow chamber (the drop down in the curves in case of Mg4Ag is caused by loss of electrical connection by hydrogen gas bubbles adhering to the surface of the specimen)*
	9	*Three MgXAg alloys showing special surface structure, SEM after 200mins electrochemistry experiment*
Tables	1	*The major components of MEM, HBSS and MEM plus (formulations offered by manufacturer)*
	2	*The information of ten commonly used biometal materials*
	3	*Surface roughness of specimens after polishing*
	4	*Table 4: Comparison of 10 commonly used metals in the MEM electrolyte.（Corrosion rate rating from high to low）*
	5	*Final potential(V) after 30 min OCP in 3 different electrolytes*
	6	The mean values±*SD of Ecorr and icorr data from 5 cycles forward and backward scan of Mg and MgXAg in HBSS, MEM and MEM+ at 37°C under flow conditions and after 30 mins*

_____

Signature, date and stamp of first supervising university professor / lecturer

_____

Signature of doctoral candidate

Journal Data Filtered By: **Selected JCR Year: 2019** Selected Editions: SCIE,SSCI
Selected Categories: **"ENGINEERING, BIOMEDICAL"** Selected Category Scheme: WoS

Gesamtanzahl: 87 Journale

Rank	Full Journal Title	Total Cites	Journal Impact Factor	Eigenfactor Score
1	Nature Biomedical Engineering	3,143	18.952	0.014180
2	Annual Review of Biomedical Engineering	4,698	15.541	0.004880
3	MEDICAL IMAGE ANALYSIS	9,028	11.148	0.017100
4	BIOMATERIALS	108,070	10.317	0.089110
5	Bioactive Materials	859	8.724	0.001650
6	Biofabrication	4,311	8.213	0.007470
7	Advanced Healthcare Materials	11,883	7.367	0.027520
8	Acta Biomaterialia	39,268	7.242	0.050720
9	npj Regenerative Medicine	417	7.021	0.001630
10	IEEE TRANSACTIONS ON MEDICAL IMAGING	21,657	6.685	0.030060
11	Bioengineering & Translational Medicine	595	6.091	0.001660
12	Photoacoustics	715	5.870	0.001760
13	Tissue Engineering Part B-Reviews	3,603	5.724	0.004190
14	IEEE TRANSACTIONS ON BIOMEDICAL ENGINEERING	23,928	4.424	0.021150
15	ARTIFICIAL INTELLIGENCE IN MEDICINE	2,953	4.383	0.003370
16	Journal of Neural Engineering	7,240	4.141	0.011940
17	Bio-Design and Manufacturing	99	4.095	0.000180
18	IEEE Transactions on Biomedical Circuits and Systems	3,534	4.042	0.006530
19	COMPUTERIZED MEDICAL IMAGING AND GRAPHICS	2,656	3.750	0.002940
20	EUROPEAN CELLS & MATERIALS	3,088	3.741	0.003140

Bioactive Materials 7 (2022) 441–452

Contents lists available at ScienceDirect

Bioactive Materials

journal homepage: www.sciencedirect.com/journal/bioactive-materials

Exploring the degradation behavior of MgXAg alloys by in vitro electrochemical methods

Yuqiuhan Zhang, Tycho Zimmermann, Wolf-Dieter Mueller *, Frank Witte, Florian Beuer, Andreas Schwitalla

Charité – Universitätsmedizin Berlin, corporate member of Freie Universität Berlin and Humboldt-Universität zu Berlin, Dental Materials and Biomaterial Research, Department of Prosthodontics, Geriatric Dentistry and Craniomandibular Disorders, Aßmannshauser Str. 4-6, 14197, Berlin, Germany

ARTICLE INFO

Keywords:
Biodegradable magnesium
Magnesium silver alloys
Electrochemistry
Hydrogen evolution

ABSTRACT

Magnesium as biodegradable biomaterial could serve as bone augmentation material in implant dentistry. The knowledge about the predictability of the biodegradation process is essential as this process needs to go hand in hand with the formation of new bone to gradually replace the augmentation material. Therefore, this work aimed to assess if the electrochemistry (EC) measurements of the corrosion process correlate with the surface features at various time points during the surface degradation, in order to describe the degradation process of Mg and Mg alloys more reliably, under the assumption that differences in EC behavior can be detected and related to specific patterns on the surface.

In this test setup, a special optical chamber was used for electrochemical measurements on Mg and Mg-alloys (Mg2Ag, Mg4Ag, and Mg6Ag). Specimens were investigated using different circulating cell culture solutions as electrolytes, these were minimum essential medium (MEM), Hank's Balanced Salt Solution (HBSS), and MEM+ (MEM with added sodium hydrogen carbonate) at 37 °C. Open circuit potential measurements (OCP) over 30 min followed by cyclic polarization were performed. The electrochemistry data, including OCP, exchange current density and corrosion potential, were compared with visible changes at the surface during these treatments over time. The results show that the addition of silver (Ag) leads to a "standardization" of the degradation regardless of the selected test medium. It is currently difficult to correlate the visible microscopic changes with the data taken from the measurements. Therefore, further investigations are necessary.

1. Introduction

Magnesium used as a base metal for implantable devices has a number of favorable properties such as a low density, the possibility to manufacture tiny structures, easiness of manipulation during surgery, the properties of its degradation products (Mg^{2+}ions) to promote the deposition of calcium and phosphorus and the growth of compact bones [1] as well as its complete degradation and absorption, making a second operation unnecessary, e.g. when used as osteosynthesis material [2].

Compared to other biodegradable metals like zinc or iron, magnesium is chemically more reactive. The rapid degradation in a humid physiological environment remains the main obstacle to widespread use, as it leads to rapid loss of mechanical integrity followed by the structural collapse of the magnesium-based implant, possibly even before the bone has healed to a structurally sound degree [3,4].

Magnesium and Mg-alloys preferentially degrade non-uniformly [5]. This is due to a complex degradation behavior and is based on the galvanic coupling occurring where the anodic and the cathodic partial reaction of the redox-reaction system take place on the same surface area [6]. The consequence thereof is, that over the surface in contact with the electrolyte (the body fluid or simulated body fluid) one part of the surface is oxidized and degraded due to the anodic reaction (1), while the two electrons are transferred to the cathodic partial reaction, where hydrogen evolution (HE) takes place (2). The Hydrogen evolution reaction (HER) is the main cathodic reaction during magnesium corrosion and occurs spontaneously [30–32]. Furthermore, the overall reaction consumes H^+ ions causing a higher concentration of OH^- ions (3), thus an increased pH in the physiological electrolyte, causing

Peer review under responsibility of KeAi Communications Co., Ltd.
* Corresponding author.
E-mail addresses: yuqiuhan.zhang@charite.de (Y. Zhang), tycho.zimmermann@charite.de (T. Zimmermann), wolf-dieter.mueller@charite.de (W.-D. Mueller), frank.witte@charite.de (F. Witte), florian.beuer@charite.de (F. Beuer), andreas.schwitalla@charite.de (A. Schwitalla).

https://doi.org/10.1016/j.bioactmat.2021.05.044
Received 21 November 2020; Received in revised form 3 May 2021; Accepted 26 May 2021
Available online 10 June 2021

Table 1
The major components of MEM, HBSS and MEM plus (formulations offered by manufacturer).

	MEM (g/L)	HBSS (g/L)	MEM Plus (g/L)
NaCl	6.8	8	6.68
$CaCl_2$	0.2	0.14	0.2
KCl	0.4	0.4	0.4
$CaCl_2$	0.2	0.14	0.2
$MgSO_4$	0.97	0.098	0.2
NaH_2PO_4	0.14	0.06	0.14
	w/o Phenol red	w/o Phenol red	w/o Phenol red
Special additives	Vitamins Amino acids w/ o$NaHCO_3$	w/o Amino acids $NaHCO_3$ 0.35 KH_2PO_4 0.06 $MgCl_2$ 1.0	Vitamins Amino acids +0.35 g/L $NaHCO_3$

precipitation of magnesium phosphate and carbonate [7]. In the next step, the dissolved Mg^+ and the OH^- ions precipitate as magnesium hydroxide layer on the surface of the Mg or Mg alloys (4) [5,8].

$$2Mg \rightarrow 2Mg^+ + e^- \text{(anodic partial reaction)} \quad (1)$$

$$2H^+ + 2e^- \rightarrow H_2 \text{ (cathodic partial reaction)} \quad (2)$$

$$2Mg + 2H^+ + 2H_2O \rightarrow 2Mg^{2+} + 2OH^- + 2H_2 \text{ (overall reaction)} \quad (3)$$

$$Mg^{2+} + 2OH^- \rightarrow Mg(OH)_2 \text{ (product formation, hydroxide layer)} \quad (4)$$

$$Mg(OH)_2 + 2Cl^- \rightarrow MgCl_2 + 2OH^- \quad (5)$$

Silver has been used by humans for thousands of years due to its strong antibacterial effects. Already under Alexander the Great's reign, silver vessels were used to store drinking water and food [9]. The formulation of silver has evolved from bulk silver in vessels and coins to ionic silver supplemented as silver salts (such as $AgNO_3$) or adsorbed on carrier materials [10]. Silver exhibits low toxicity in the human body, and minimal risk is expected due to clinical exposure by inhalation, ingestion, dermal application or through the urological or hematogenous route [11]. Innovative binary Mg–Ag alloys were built as bone implant material to add antibacterial properties to biodegradable magnesium. When combined with its propensity to degrade in physiological conditions, the antibacterial property may last for the duration of the implant. Among the criteria for determining biocompatibility and antibacterial reaction [12], the various corrosion rates from αand β phases influence the corrosion mechanism [13]. The corrosion potential of Mg–Ag metal compounds is shifted in an anodic direction by adding silver. Because these complex interactions remain a critical concern, it is important to explore the corrosion behavior of magnesium-silver alloys in detail [14,15].

For in vitro experiments to study the biodegradation of Mg and Mg alloys, various types of simulated body fluids have been used [27,28]. So far, there is no clear consensus on the best type of environment to simulate physiological in vivo conditions [16]. The corrosive environment of Mg in the human body is composed of 0.14 M NaCl solution and a small amount of other inorganic substances (such as Ca^{2+}, PO_4^{3-} and HCO^{3-}) [17]. The normal pH of blood is 7.4, generally buffered by the CO_2/HCO_3^- system [18]. The presence of chloride ions usually leads to accelerated corrosion [19], since the formation of $MgCl_2$ releases OH^- ions from the precipitation layer (5), which in turn can react with the

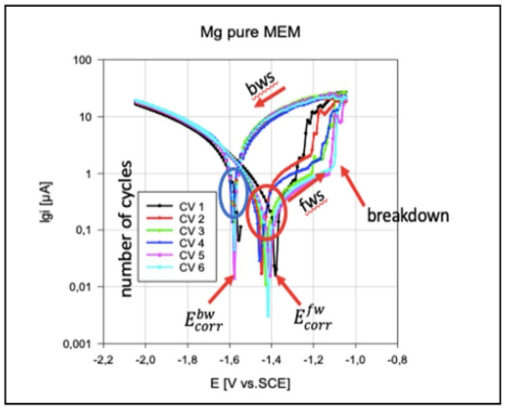

Fig. 2. Description of I vs. E curves (The blue circle marks the range of backward scan for assessing I_{corr}, the red circle for the forward scan and the red arrows marked the scan direction and points of interest.). (For interpretation of the references to color in this figure legend, the reader is referred to the Web version of this article.)

Table 2
Surface roughness of specimens after polishing.

materials	Sa (left)	Sa (right)	Sa (up)	Sa (down)	Sa (middle)	±SD (Sa)
Mg2Ag (µm)	1.426	1.688	1.706	1.523	1.747	0.1371
Mg4Ag (µm)	1.018	1.233	0.963	1.034	1.187	0.1163
Mg6Ag (µm)	1.352	0.932	1.097	0.908	1.138	0.1796
Mg XHP	1.316	1.313	1.337	1.328	1.329	0.0099
Mg Pure	1.341	1.298	1.327	1.305	1.315	0.0172

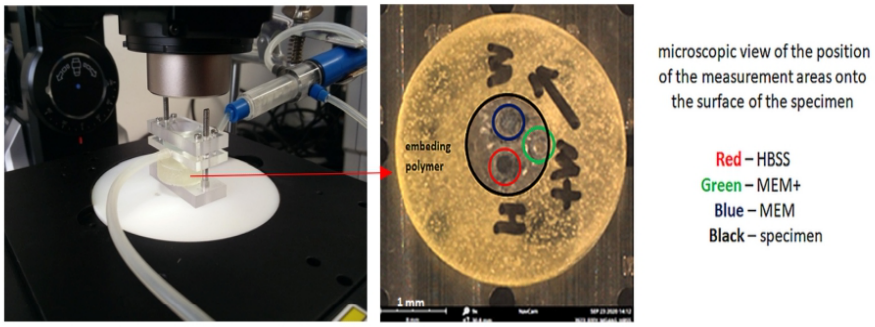

Fig. 1. left: electrochemical flow chamber under the video-microscope (magnification x135) right: the measurement areas on the surface of the specimen for each of the electrolytes.

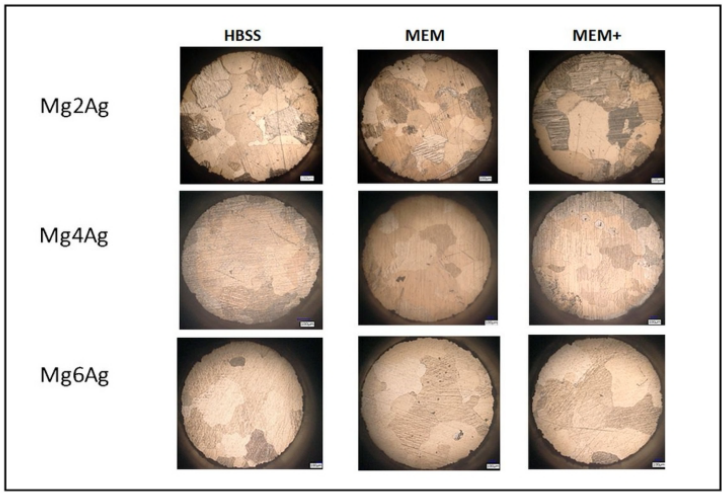

Fig. 3. Initial states of MgXAg alloys before the electrochemical measurements in HBSS – MEM and MEM+.

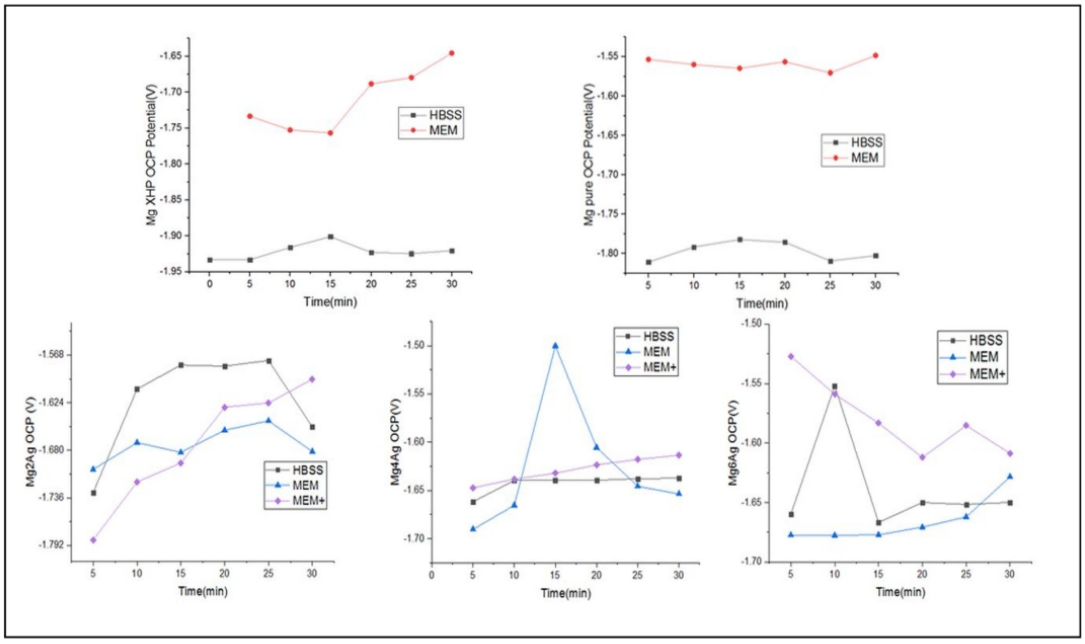

Fig. 4. Comparison of the OCP vs. time curves of Mg XHP and Mg pure on the top and MgXAg (from left to right: 2Ag, 4Ag, 6Ag) in MEM, HBSS and MEM + at 37 °C in a flow chamber.

Table 3
Final potential(V) after 30 min OCP in 3 different electrolytes.

Mg/Mg alloys	Mg XHP	Mg pure	Mg2Ag	Mg4Ag	Mg6Ag
HBSS	−1.920	−1.802	−1.652	−1.637	−1.649
MEM	−1.645	−1.768	−1.681	−1.653	−1.628
MEM+			−1.596	−1.613	−1.608

dissolved Mg^{2+} ions, while phosphates and carbonates may promote the formation of protective or partially protective corrosion products [12]. The presence of organic components, such as proteins, cells, or bacteria, can additionally affect the corrosion reaction [20]. Compared to room temperature, the body temperature of 37 °C can accelerate the corrosion reaction on the one hand and modify it to some extent on the other, since the solubility of calcium phosphate is also dependent on the temperature

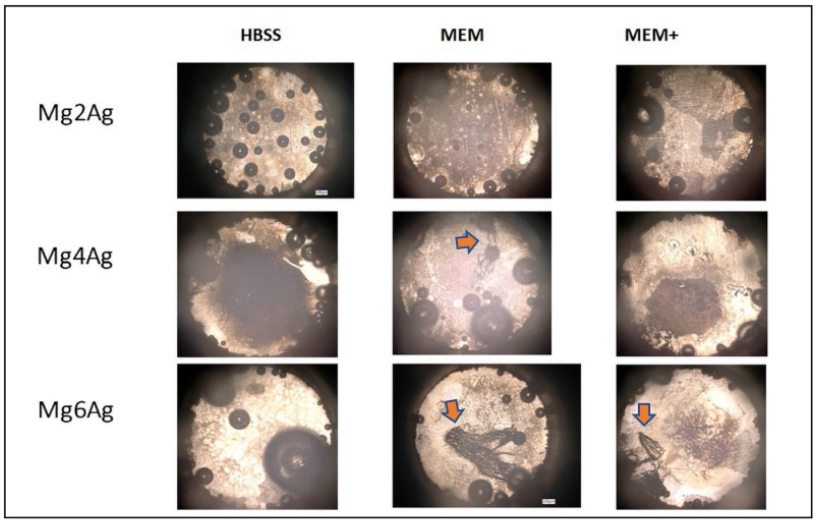

Fig. 5. situation at the surface of MgXAg alloys after OCP measurements over 30 min in HBSS – MEM and MEM+. Initial degradation is marked by red arrows. (For interpretation of the references to color in this figure legend, the reader is referred to the Web version of this article.)

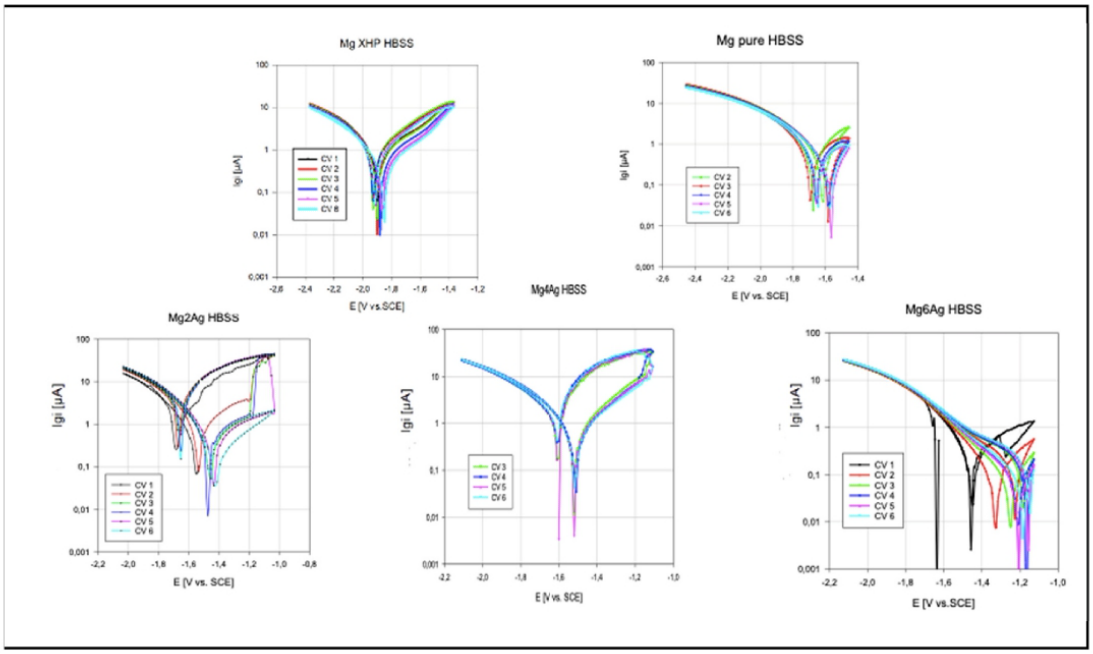

Fig. 6a. Comparison of the electrochemical behavior of Mg XHP and Mg pure in HBSS (top) and MgXAgalloys (buttom) at 37 °C in a flow chamber.

[21]. These different influencing factors deriving from the bodily environment make investigations of the corrosion process very complex and thus challenging.

The results of many literature outcomes have plainly showed that the consumption of Mg is exceptional regarding its electrochemical behavior. In nature, the corrosion of Mg and its alloys is an electrochemical process, and their corrosion performance or characteristics can be ultimately attributed to their electrochemical behavior. Revealing the electrochemical reactions involved in the corrosion process can provide a theoretical basis for understanding the characteristic corrosion phenomena for Mg and its alloys [22]. Therefore, the study aimed to correlate electrochemical (EC) measurements with surface

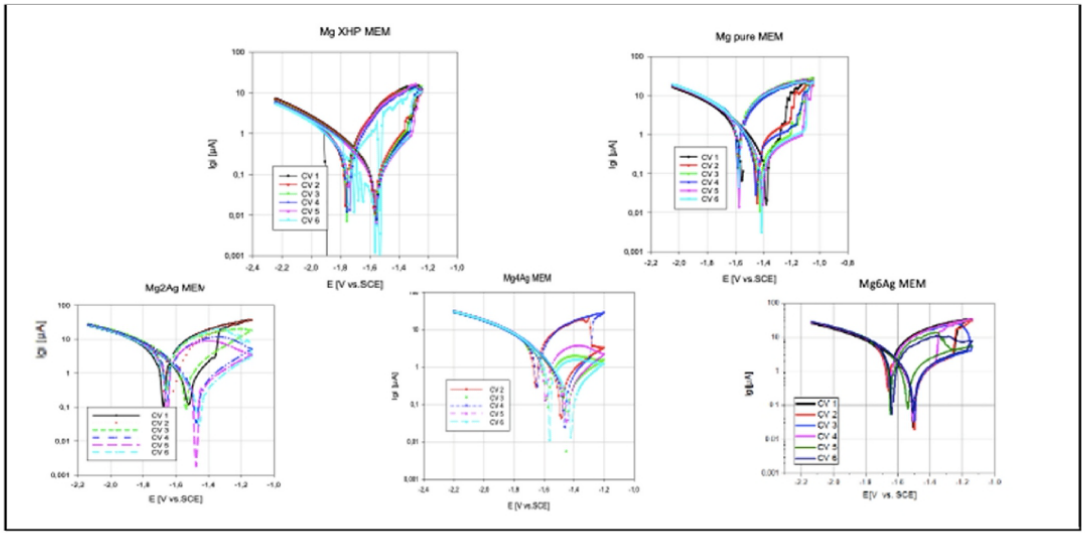

Fig. 6b. Comparison of the I vs.E curves of cyclic polarization of Mg XHP and Mg pure in MEM (top) and MgXAg alloys (bottom) at 37 °C in a flow chamber.

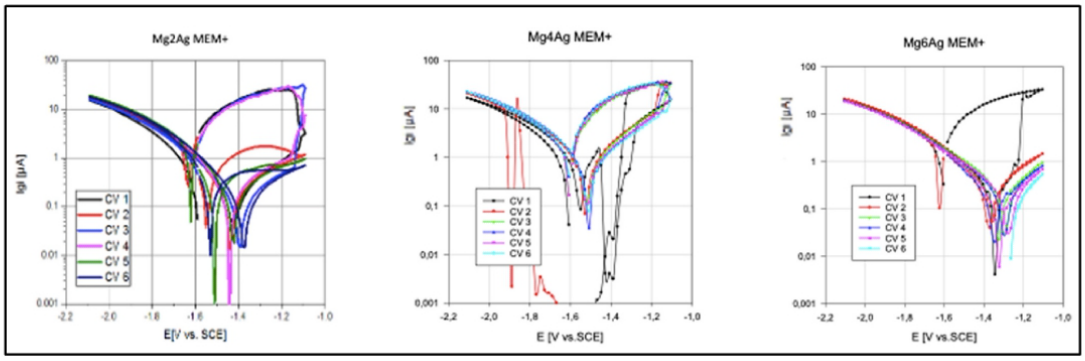

Fig. 6c. Comparison of the I vs.E curves of cyclic polarization of MgXAg in MEM + at 37 °C in a flow chamber (the drop down in the curves in case of Mg4Ag is caused by loss of electrical connection by hydrogen gas bubbles adhering to the surface of the specimen).

changes at different points in time under the influence of three different electrolytes based on the cell culture medias HBSS and MEM to predict the degradation process more reliably.

2. Material and method

In these experiments, MEM (Biochrom GmbH, Germany) and HBSS (Life Technologies Limited, UK) buffers, commonly used in the literature, were selected. In contrast to MEM, where amino acids and vitamins are added to the basic ingredients, HBSS contains additional $NaHCO_3$ (Sigma-Aldrich Chemie GmbH, Germany), as shown in Table 1. To better compare the corrosion process, in the MEM Plus group 0.35 g/L sodium bicarbonate was added.

Mg XHP (purity: 99.99%) and Mg pure (purity: 99%), as well as three Mg-Ag alloys - Mg2Ag, Mg4Ag and Mg6Ag which contain 1.87%, 3.82% and 6.00% silver and 98%, 96% and 94% magnesium by weight, respectively - were cast and processed with solution T4. All specimens were cylindrical with a diameter of 10 mm and a thickness of 5 mm. In order to describe the initial degradation process in a time frame of 1 h, an optical coupled electrochemical measurement set up was used [24].

2.1. Preparation of magnesium specimens

Mg XHP, Mg pure and MgXAg (X = 2,4,6) samples were prepared by partial encapsulation in an epoxy resin to keep the sample intact during grinding. The surface was ground from 800 till 2500 using silicon carbide sandpaper (150 mm Hermes, Germany) with water, then polished with 1.0 μm silica suspension and etched by a solution, mainly consisting of glacial acetic acid and picric acid, for 10 s for each specimen. Afterwards, the surface of the specimens was washed with ethanol and dried.

2.2. Grain size and roughness measurement

For comparison of the surface conditions the specimens were inspected using a video microscope (Keyence VHX-5000, Japan) and the

Table 4
The mean values ± SD of E_{corr} and i_{corr} data from 5 cycles forward and backward scan of Mg and MgXAg in HBSS, MEM and MEM + at 37 °C under flow conditions.

forward	I [A]	E [V vs SCE]	I [A]	E [V vs SCE]	I [A]	E [V vs SCE]
	HBSS		MEM		MEM+	
Mg2Ag	2.2 × 10^{-5} ±1.49 × 10^{-5}	−1.508 ±0,092	3.73 × 10^{-5} ±4.74 × 10^{-5}	−1.513 ±0.052	6.15 × 10^{-6} ±1.19 × 10^{-6}	−1.414 ±0.028
Mg4Ag	5.63 × 10^{-5} ±4.59 × 10^{-5}	−1.515 ±0.023	1.41 × 10^{-5} ±4.23 × 10^{-6}	−1.458 ±0.022	2.26 × 10^{-5} ±1.53 × 10^{-6}	−1.526 ±0.018
Mg6Ag	4.2 × 10^{-6} ±2.37 × 10^{-6}	−1.270 ±0.10	2.86 × 10^{-5} ±3.67 × 10^{-6}	−1.509 ±0.015	7.35 × 10^{-5} ±2.13 × 10^{-6}	−1.304 ±0.037
pure	±4.94 × 10^{-6}	−1.597	±2.65 × 10^{-5}	−1.467		
XHP	±5.48 × 10^{-6}	−1.878	±1.19 × 10^{-6}	−1.560		
backward						
Mg2Ag	8.62 × 10^{-6} ±5.44 × 10^{-6}	−1.297 ±0.07	1.27 × 10^{-5} ±4.60 × 10^{-6}	−1.435 ±0.014	5.94 × 10^{-6} ±1.88 × 10^{-6}	−1.415 ±0.02
Mg4Ag	5.59 × 10^{-5} ±2.90 × 10^{-5}	−1.419 ±0.02	7.28 × 10^{-6} ±1.93 × 10^{-6}	−1.371 ±0.019	2.4 × 10^{-5} ±5.57 × 10^{-6}	−1.495 ±0.022
Mg6Ag	1.1 × 10^{-5} ±6.41 × 10^{-6}	−1.378 ±0.04	7.4 × 10^{-5} ±1.49 × 10^{-5}	−1.493 ±0.034	5.26 × 10^{-6} ±1.30 × 10^{-6}	−1.279 ±0.042
pure	±3.30 × 10^{-6}	−1.674	±2.45 × 10^{-5}	−1.575		
XHP	±3.06 × 10^{-6}	−1.924	±1.00 × 10^{-6}	−1.751		

roughness at 5 spots of each specimen was measured using an IF-microscope (Alicona, Austria).

2.3. Electrochemical measurements

For electrochemical measurements, the specimens were connected to a copper wire using a silver amalgam. The reactions at the surface of the specimens were observed using a video microscope (Keyence VHX-5000) through a special electrochemical cell [24] (Fig. 1). The electrochemical data were manipulated and accumulated by the software PStrace (PalmSens, Netherlands) connected to a mini-potentiostat (Emstat3+, PalmSens, Netherlands). The solutions were pumped through the system using a lab pump (Watson Marlow 5050Di, United Kingdom). The speed was set as 4.3 ml/min and the temperature was set to 37 °C (310K). The OCP (open circuit potential) was measured over 30min followed by cyclic polarization over 6 cycles between a potential range of ±500 mV vs. OCP (open circuit potential). The microscopic video observations during the measurements were recorded with OBS Studio (version 26.0.2). Scanning Electron Microscope (SEM) pictures were made by Desktop SEM Phenom XL G2 (Thermo Fisher Scientific, America). The specimens were washed in pure alcohol and blow dried before SEM.

2.4. Data collection and analysis

From each of the cyclic I-E curve the exchange current density i_{corr} was determined at $E_{corr.}$ The body temperature of 310K, the number of the transferred electrons per reaction (n = 2), the Faraday's constant F with ·96485 As·mol^{-1} as well as the Stern-Geary-Coefficient with 0.01335 were used in equation (6), the linearized Butler-Volmer equation.

$$I_0 = \frac{RT}{nFR_p} = \frac{Stern - Geary - Coefficient}{R_p} (A/cm^2) \quad (6)$$

One example of a specific I vs E cyclic curve with the marked data points is shown in Fig. 2.

3. Results

3.1. Roughness measurements

The roughness values of the investigated specimens are comparable, as the data show in Table 2. Mg2Ag shows the highest roughness followed by both pure Mg specimens and then Mg4Ag and Mg6Ag.

The pictures in Fig. 3 show the initial states of the surface of the MgXAg alloys prepared for the electrochemical measurements in HBSS, MEM and MEM+.

3.2. Electrochemical measurements

In all cases the OCP values starts from a very cathodic point and after the first 5 min reach a value which was more or less constant over the rest of the measurement time up to 30 min as shown for the different investigated alloys in Fig. 4.

Contrary to expectations, no major differences were found for the OCP for the MgXAg alloys. Only in case of the pure and ultra-pure Mg it can be seen that the OCP after 30 min in MEM is more anodically shifted in comparison to HBSS. The final potentials after 30 min are summarized in Table 3.

The situation at the surface after 30min OCP is shown in Fig. 5.

Even if the OCP values hardly differ, the images show visible differences after 30 min, as seen in Fig. 5. In HBSS, a difference in the amount and distribution of the HE spots and the oxide-covered area can

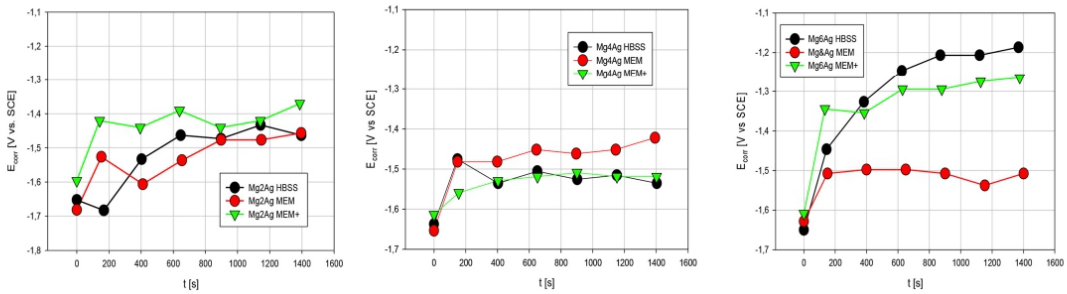

Fig. 7. Changes of E_{corr} of the forward scan with time for MgXAg alloys in 3 different electrolytes at 37 °C und flowing conditions.

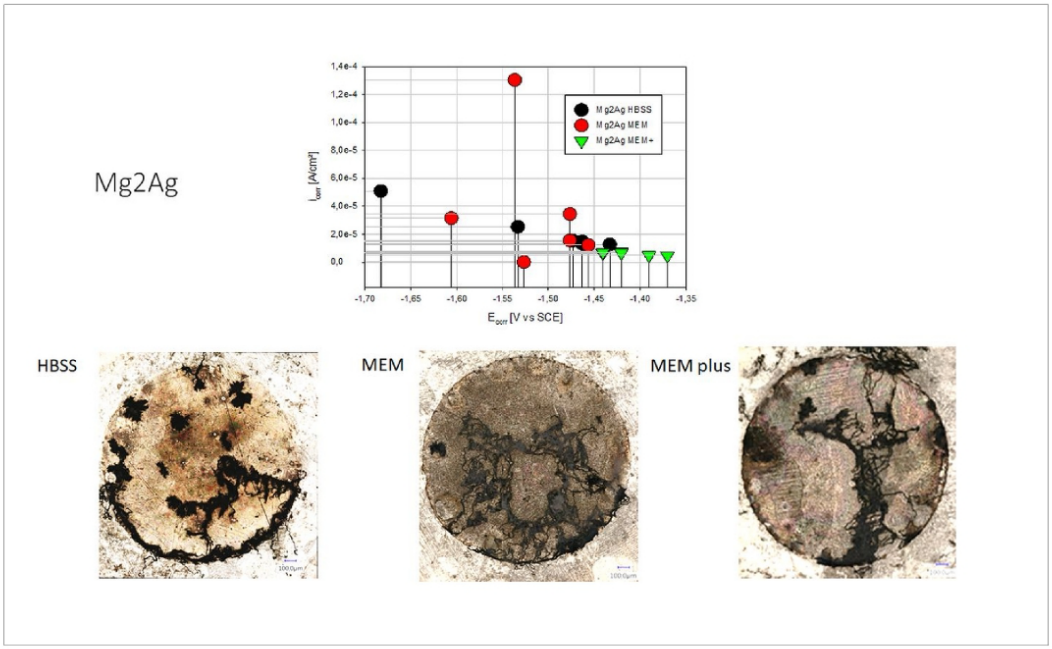

Fig. 8a. Comparison of i_{corr} vs. E_{corr} data from cyclic polarization (top) of Mg2Ag alloy in HBSS, MEM and MEM + together with the situation at the surface after the electrochemical measurements.

be observed. In MEM all surfaces show strong traces of oxidation, either through dark discoloration, as in the case of Mg2Ag, or paths of localized "migrating" reactions, marked with red arrows, on Mg4Ag and Mg6Ag. If $NaHCO_3$ is added to the MEM solution, the initial traces of localized oxidation are less clear and can only be seen on Mg6Ag.

3.2.1. Cyclic voltammetry

The cyclic voltammograms show different shapes, depending on the kind of solution as well as the kind of material, pure Mg or MgXAg alloys. There are differences related to the position of the E_{corr} and the i_{corr} data depending on the solution in which was measured. In case of the pure and ultra-pure Mg the behavior under cyclic polarization is completely different, as the curves in Fig. 6a show. In HBSS, pure Mg as well as MgXHP show no breakdown, so no additional HE (Hydrogen evolution) takes place during anodic polarization, but in MEM the typical behavior can be observed with fast hydrogen streams at some places at the surface. Characteristically, very small bubbles are created, appearing as a little stream.

In Fig. 6a to c the curves of the differently composed MgXAg alloys, polarized in different electrolytes are presented. Depending on the Ag-content some differences in the behavior can be observed. Phenomenologically, the behavior in HBSS and MEM + are comparable but slightly different to the behavior in MEM. The CV of the alloys tested in MEM (Fig. 6b) indicate that magnesium and Mg–Ag alloys exhibit hysteresis. This suggests that the material experienced pitting corrosion to some degree during immersion in the electrolytes. It is important to realize that as more silver content is included, the alloys become more prone to pitting corrosion. However, this seems to be suppressed again by adding $NaHCO_3$, as can be seen in Fig. 6c. Mg6Ag shows pitting corrosion behavior only in the first cycle but with the passing of time, respectively the numbers of cycles, a decrease of corrosion current can be observed.

The essential data of the E_{corr} position of the forward and backward scans and the i_{corr} data respectively are presented in Table 4.

Fig. 7 shows the changes of E_{corr} depending on time, which is also related to the numbers of cycles.

In all cases an anodic shift of E_{corr} with time can be observed. Hereby the clear anodic shift of Ecorr for Mg6Ag in $NaHCO_3$ containing electrolytes is surprising.

The data show also, that at anodically shifted E_{corr} potentials the values of i_{corr} are significantly lower as in case of more cathodically located ones, as exemplified in Fig. 8a–c.

Fig. 8a to c show the surfaces after the electrochemical polarization.

After the treatment, clear changes can be seen on the surfaces, with one exception, Mg6Ag in HBSS. There are clear traces of localized "moving" oxidation reactions, impressing as black, meandering lines. In the case of Mg4Ag in MEM plus, the areas of pitting, typical for static electrolytes, can be seen. Mg6Ag in HBSS surprises with an almost even coverage of the surface with an oxide layer without noticeable degradation spots.

3.3. Scanning electron-microscopy (SEM)

The SEM images (Fig. 9) of MgXAg show the surface of the specimens in three kinds of electrolytes after 200 min of electrochemical testing. MgO and $Mg(OH)_2$ are the main corrosion products around pits and cracks [25]. After electrochemical testing, all three alloys showed an irregularly spaced non-circular concavity pattern, all exhibiting a depressed surface. Mg2Ag showed both homogeneous and pitting corrosion, while Mg6Ag exhibit only mild and evenly distributed signs of pitting corrosion compared with the other two alloys in the same electrolytes. When $NaHCO_3$ is added to the MEM electrolyte with the same alloy, larger pits are clearly formed.

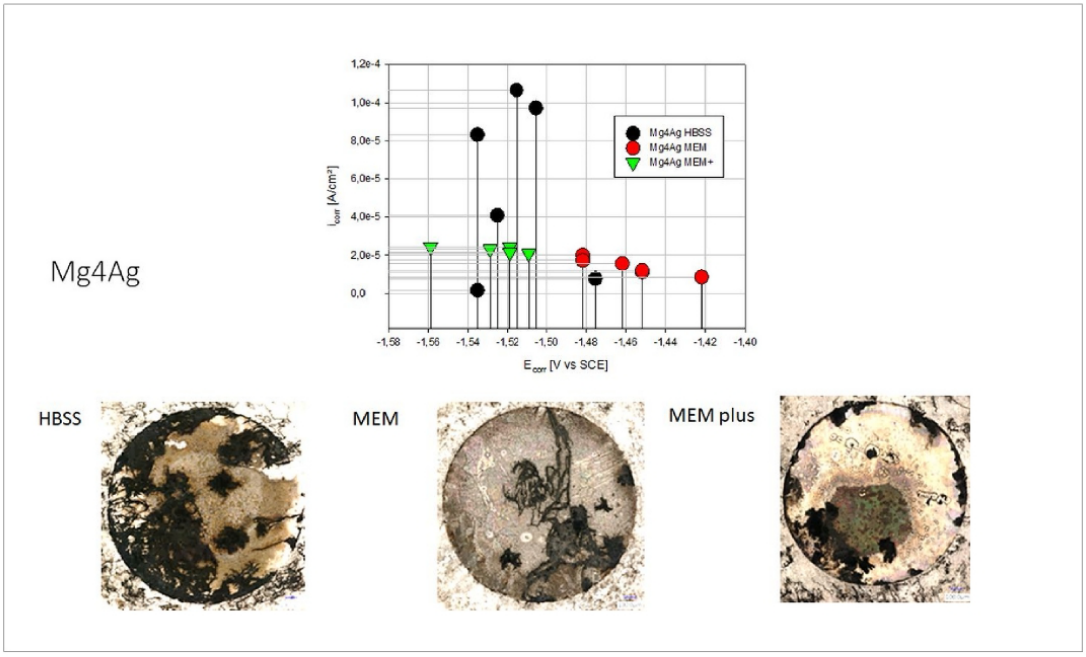

Fig. 8b. Comparison of i_{corr} vs. E_{corr} data from cyclic polarization (top) of Mg4Ag alloy in HBSS, MEM and MEM + together with the situation at the surface after the electrochemical measurements.

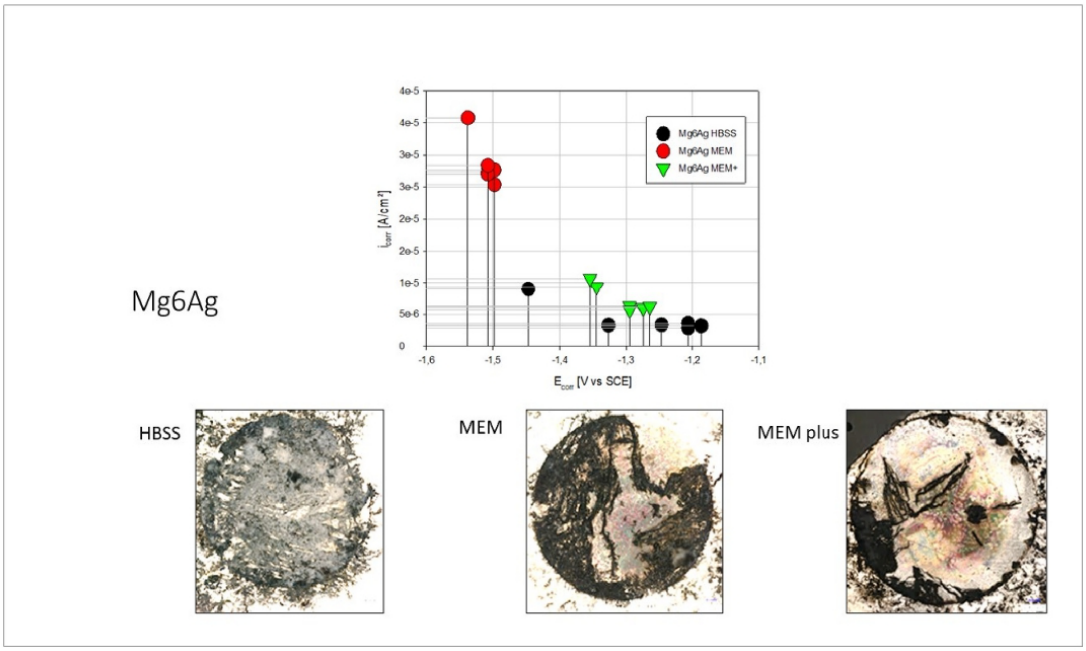

Fig. 8c. Comparison of i_{corr} vs. E_{corr} data from cyclic polarization (top) of Mg6Ag alloy in HBSS, MEM and MEM + together with the situation at the surface after the electrochemical measurements. The video microscopic view before (left) Mag: x = 150 and after (right) Mag.: x = 300; 2.5 h after the end of the experiment.

448

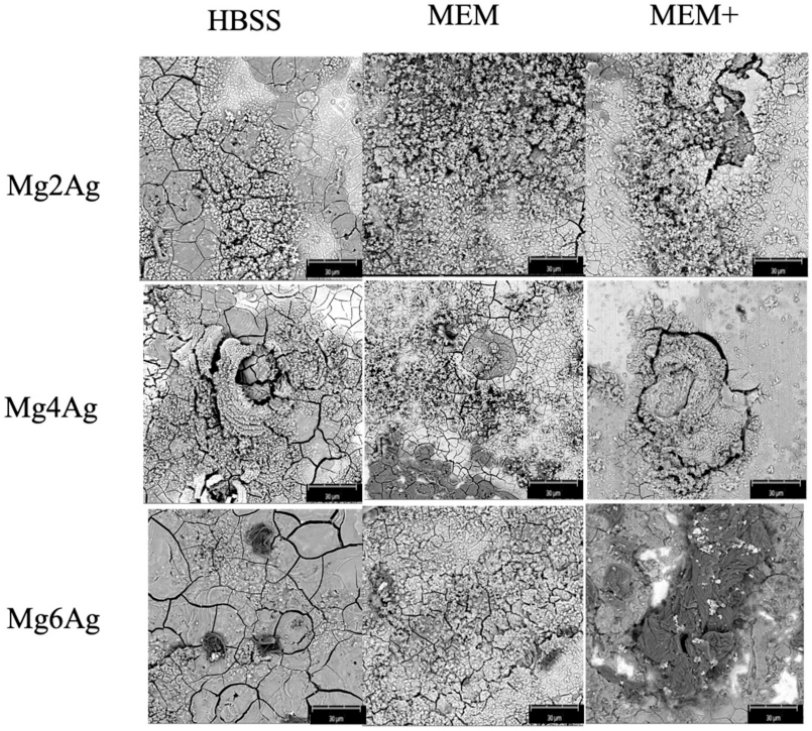

Fig. 9. Three MgXAg alloys showing special surface structure, SEM after 200mins electrochemistry experiment.

4. Discussion

The exchange current densities of (i_{corr} or i_0) represent intrinsic electron transfer rates between an analyte and an electrode [26]. These rates give insights into the composition of the analyte and the electrode and their interactions. In order to fully understand the degradation mechanism of magnesium and its alloys, the excess of HE over the Mg surface should be quantified [23].

Based on our question and aim, we expected to find a reliable correlation between the electrochemical behavior, especially when examining the exchange current density which describes the degradation rate in in-vitro environment, and the composition of the electrolytes. Secondly, we expected to investigate the influence of the visible changes including the hydrogen evolution and degradation product deposition at the surface by optical inspection during open circuit degradation and electrochemical polarization of MgXAg alloys [14,15].

As the here presented data show, a difference in the electrochemical behavior of Mg XHP and Mg pure depending on the used in-vitro solutions, HBSS and MEM, exists. To simulate the CO_2 buffer activity in MEM for the measurements of the MgXAg alloys a third electrolyte, MEM+, was used.

The measurements performed in this experiment didn't clearly show any systematic factor for the difference in electrochemical behavior for MgXAg alloys. A comparison of the optical recordings before and after polarization (cyclic voltammetry) shows that a surface that is already showing active corrosion is then attacked to a greater extent. An initially only slightly oxidized surface can, however, be changed dramatically by the polarization.

This can be explained by various influences, based on the alloy composition and its structure, such as the grain sizes and orientation as well as the chemical activity [29].

Based on our observation, no specific spots could be detected which could be fitted to the hydrogen evolution or the oxidation and precipitation of less soluble products at the surface. All analyzed surfaces have shown their own specific structure, which can be seen at the end of the treatment in Fig. 8a–c.

On the freshly polished Mg surface exposed to an aqueous solution (such as MEM or HBSS solution), corrosion proceeds on the edge of the growing patch, thereby causing the corrosion product to precipitate in the vicinity. Magnesium corrosion products have shown enhanced catalytic activity for HER [13–15].

Using the possibility to assess the forward as well as the backward scan for description of the electrochemical activity of the different MgXAg alloys, it can be shown that a slight relation between the Ag content and the anodic shift of E_{corr} at the height of i_{corr} can be seen. In case of Mg6Ag, the CO_2 containing electrolytes, HBSS and MEM+, show the same activity, in contrast to CO_2-free electrolyte (MEM). But in case of Mg2Ag and Mg4Ag it is not detectable, as Fig. 10a and b show.

In every investigated case, a kind of pitting corrosion as the main form of degradation was observed at the end and it can be seen in the SEM pictures, Fig. 9. The inhomogeneity of the metal surface is one important cause of pitting corrosion [33]. The chloride ion concentration in the solution accelerates the degradation [19].

For the electrochemical assessment of the degradation of Mg and Mg-alloys these conditions are confounding [34,35]. The reduction of active reaction area as well as the link between anodic and cathodic reaction pathways make a prediction of degradation more complicated. The application of the video-optical set-up gives more information regarding

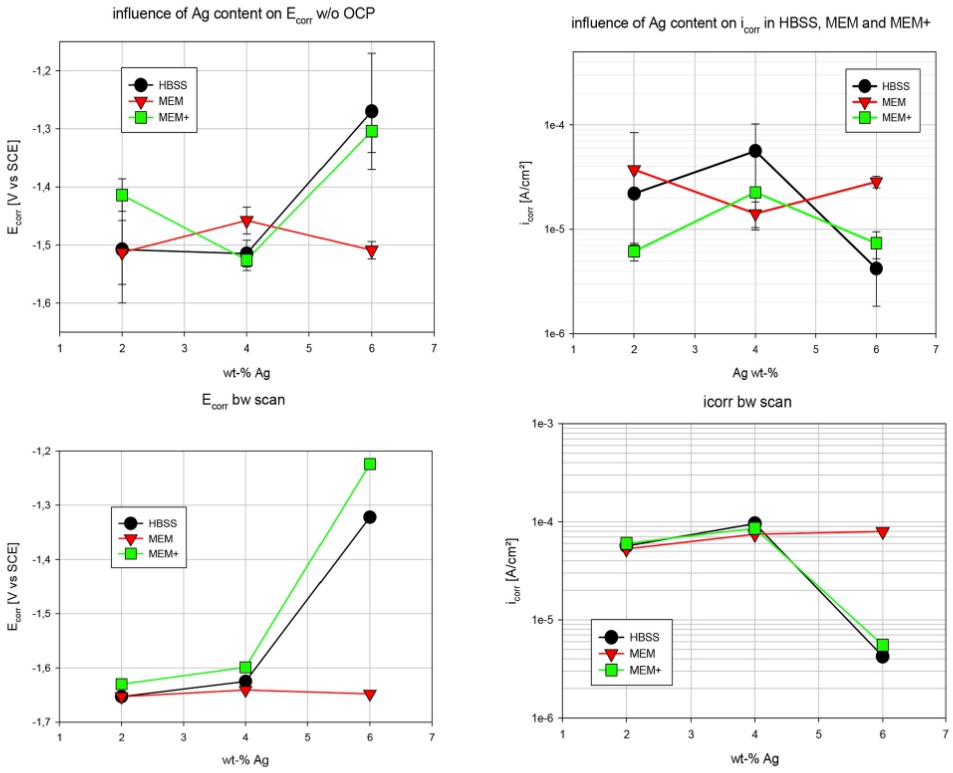

Fig. 10. Assessment of forward (top) and backward (bottom) scan for 3 different MgXAg alloys in 3 different electrolytes.

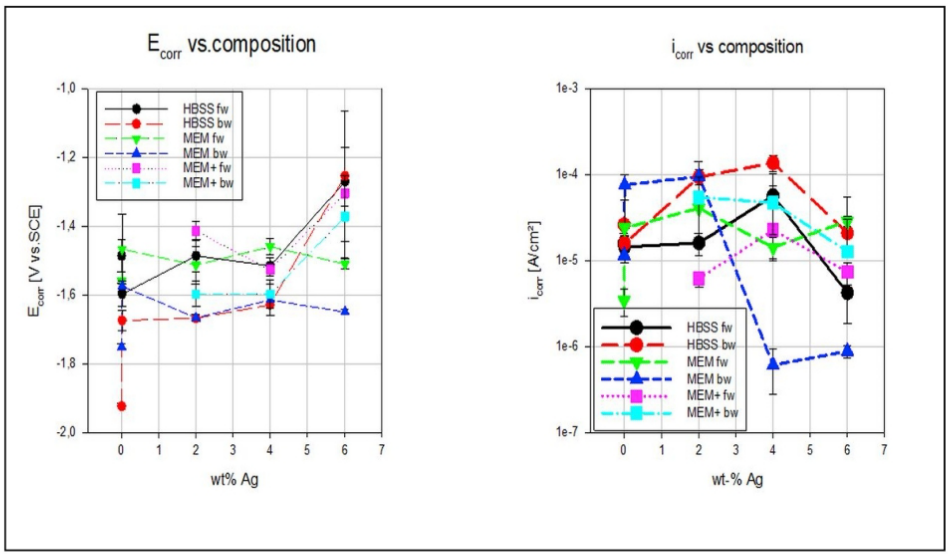

Fig. 11. Influence of the Ag-content on E_{corr} (left) and i_{corr} (right). Comparison of the data from cyclic voltammetry divided into forward and backward scan.

the influence of the composition of the electrolyte on the degradation behavior of MgXAg alloys, because the pictures during the investigation were different, namely changing positions of the oxidation, the above-mentioned meandering black lines, and also fixed positions for the hydrogen formation in the vicinity of which no visible change in the surface appearance were detected.

This makes it difficult to get a reliable picture of the degradation of Mg and Mg alloys. The visible changes on the surfaces impressed in some cases as a strong degradation and modification of the surface were not well expressed in the electrochemical data, as summarized in Fig. 11.

Due to the galvanically coupled reaction on the surface, only a trend of degradation can be given. There are more experiments necessary to find the key effect or the key location(s) of surface changes, which can be correlated to the measured electrochemical activity.

5. Conclusion

The varying rates of corrosion from one phase to another influenced the mechanism of pitting corrosion. The corrosion potential of Mg–Ag metallic compounds was moved in anodic direction by adding silver content. The composition of the alloy as well as the composition of the electrolyte have a significant influence on the electrochemical performance of the investigated alloys.

Most interestingly, we discovered that the silver content is a critical element in pitting corrosion protection of magnesium alloys while keeping the overall corrosion rate under control. It is also vital to pay more attention to the concept of protein evoked effects during magnesium corrosion, as it undoubtedly plays an important role in reducing both homogeneous and pitting corrosion of magnesium materials used in the body. Dependent on this performance, biodegradable implants containing MgXAg binary alloys would have a multifunctional use. In the next step the observation period can be extended, or the pH changed to monitor changes in the magnesium corrosion site. It is also our aim to track the factors influencing the trend of pitting corrosion during the reaction.

CRediT authorship contribution statement

Yuqiuhan Zhang: Conceptualization, Methodology, Formal analysis, Writing – original draft, Writing – review & editing, Visualization, Validation, Formal analysis, Investigation. **Tycho Zimmermann:** Conceptualization, Methodology, Formal analysis, Writing – review & editing. **Wolf-Dieter Mueller:** Conceptualization, Formal analysis, Resources, Visualization, Writing – review & editing, Writing – original draft, Supervision, Project administration. **Frank Witte:** Resources, Project administration. **Florian Beuer:** Resources, Supervision, Project administration. **Andreas Schwitalla:** Supervision, Project administration, Review & Editing.

Declaration of competing interest

The authors declare that they have no known competing for financial interests or personal relationships that could have appeared to influence the work reported in this paper.

Acknowledgement

The authors would like to thank Dr. N. Hort from HZG for delivering the MgXAg specimens and Prof. Uggowitzer ETH Zurich for offering the Mg XHP and Mg pure.

References

[1] G.Y. Liu, J. Hu, Z.K. Ding, C. Wang, Bioactive calcium phosphate coating formed on micro-arc oxidized magnesium by chemical deposition, Appl. Surf. Sci. 257 (6) (2011) 2051–2057, https://doi.org/10.1016/j.apsusc.2010.09.050.

[2] C. Janning, et al., Magnesium hydroxide temporarily enhancing osteoblast activity and decreasing the osteoclast number in peri-implant bone remodelling, Acta Biomater. 6 (5) (2010) 1861–1868, https://doi.org/10.1016/j.actbio.2009.12.037.

[3] F. Witte, Acta Biomaterialia the history of biodegradable magnesium implants : a review q, Acta Biomater. 6 (5) (2010) 1680–1692, https://doi.org/10.1016/j.actbio.2010.02.028.

[4] H.S. Brar, M.O. Platt, M. Sarntinoranont, P.I. Martin, M.V. Manuel, Magnesium as a biodegradable and bioabsorbable material for medical implants, Jom 61 (9) (2009) 31–34, https://doi.org/10.1007/s11837-009-0129-0.

[5] B.G. Song, A. Atrens, Understanding magnesium corrosion A framework for improved alloy performance **, 2003, pp. 837–858, https://doi.org/10.1002/adem.200310405, 12.

[6] H. Wu, et al., Crevice corrosion – a newly observed mechanism of degradation in biomedical magnesium, Acta Biomater. 98 (2019) 152–159, https://doi.org/10.1016/j.actbio.2019.06.013.

[7] Y. Xin, K. Huo, H. Tao, G. Tang, P.K. Chu, Influence of aggressive ions on the degradation behavior of biomedical magnesium alloy in physiological environment, Acta Biomater. 4 (6) (2008) 2008–2015, https://doi.org/10.1016/j.actbio.2008.05.014.

[8] Z. Shi, J.X. Jia, A. Atrens, Galvanostatic anodic polarisation curves and galvanic corrosion of high purity Mg in 3 . 5 % NaCl saturated with Mg (OH) 2, Corrosion Sci. 60 (2012) 296–308, https://doi.org/10.1016/j.corsci.2011.12.002.

[9] S. Silver, L.T. Phung, G. Silver, Silver as biocides in burn and wound dressings and bacterial resistance to silver compounds, J. Ind. Microbiol. Biotechnol. 33 (7) (2006) 627–634, https://doi.org/10.1007/s10295-006-0139-7.

[10] B. Kwakye-Awuah, C. Williams, M.A. Kenward, I. Radecka, Antimicrobial action and efficiency of silver-loaded zeolite X, J. Appl. Microbiol. 104 (5) (2008) 1516–1524, https://doi.org/10.1111/j.1365-2672.2007.03673.x.

[11] A.B.G. Lansdown, Silver in health care: antimicrobial effects and safety in use interactions between skin and biofunctional metals, Curr. Probl. Dermatol. 33 (2006) 17–34.

[12] X. Gu, Y. Zheng, Y. Cheng, S. Zhong, T. Xi, Biomaterials in vitro corrosion and biocompatibility of binary magnesium alloys, Biomaterials 30 (4) (2009) 484–498, https://doi.org/10.1016/j.biomaterials.2008.10.021.

[13] Y.H. Kim, et al., The effect of ball milling on the pH of Mg-based metals, oxides and Zn in aqueous media, Met. Mater. Int. 16 (2) (2010) 253–258, https://doi.org/10.1007/s12540-010-0414-z.

[14] G. Song, Control of biodegradation of biocompatable magnesium alloys 49 (2007) 1696–1701, https://doi.org/10.1016/j.corsci.2007.01.001.

[15] P. Rosemann, J. Schmidt, A. Heyn, Short and long term degradation behaviour of Mg-1Ca magnesium alloys and protective coatings based on plasma-chemical oxidation and biodegradable polymer coating in synthetic body fluid, Mater. Corros. 64 (8) (2013) 714–722, https://doi.org/10.1002/maco.201206590.

[16] N. Ahmad, F. Feyerabend, B. Mihailova, S. Heidrich, U. Bismayer, R. Willumeit-römer, Magnesium degradation in fl uenced by buffering salts in concentrations typical of in vitro and in vivo models, Mater. Sci. Eng. C 58 (2016) 817–825, https://doi.org/10.1016/j.msec.2015.09.067.

[17] S. Virtanen, I. Milošev, E. Gomez-Barrena, R. Trebše, J. Salo, Y.T. Konttinen, Special modes of corrosion under physiological and simulated physiological conditions, Acta Biomater. 4 (3) (2008) 468–476, https://doi.org/10.1016/j.actbio.2007.12.003.

[18] A. Witecka, et al., In vitro degradation of ZM21 magnesium alloy in simulated body fluids, Mater. Sci. Eng. C 65 (2016) 59–69, https://doi.org/10.1016/j.msec.2016.04.019.

[19] C. Taltavull, Z. Shi, B. Torres, J. Rams, A. Atrens, Influence of the chloride ion concentration on the corrosion of high-purity Mg , ZE41 and AZ91 in buffered Hank ' s solution. ", 2014, pp. 329–345, https://doi.org/10.1007/s10856-013-5087-y.

[20] D. Hong, et al., Controlling magnesium corrosion and degradation-regulating mineralization using matrix GLA protein, Acta Biomater. 98 (2019) 142–151, https://doi.org/10.1016/j.actbio.2019.05.048.

[21] M. Sumita, T. Hanawa, I. Ohnishi, Failure processes in biometallic materials, Compr. Struct. Integr. (2003) 131–167.

[22] G. Song, Corrosion Electrochemistry of Magnesium (Mg) and its Alloys, Woodhead Publishing Limited, 2011.

[23] Y. Yang, F. Scenini, M. Curioni, Electrochimica Acta A study on magnesium corrosion by real-time imaging and electrochemical methods : relationship between local processes and hydrogen evolution, Electrochim. Acta 198 (2016) 174–184, https://doi.org/10.1016/j.electacta.2016.03.043.

[24] T. Zimmermann, N. Hort, Y. Zhang, W.D. Müller, A. Schwitalla, The video microscopy-linked electrochemical cell: an innovative method to improve electrochemical investigations of biodegradable metals, Materials (Basel). 14 (7) (2021), https://doi.org/10.3390/ma14071601.

[25] D. Tie, et al., In vitro mechanical and corrosion properties of biodegradable Mg – Ag alloys, 2014, pp. 569–576, https://doi.org/10.1002/maco.201206903, 6.

[26] R. G. Kelly, J. R. Scully, D. W. Shoesmith, and R. G. Buchheit, Electrochemical Techniques in Corrosion Science and Engineering.. .

[27] D. Tie, F. Feyerabend, W. Müller, R. Schade, K. Liefeith, K.U. Kainer, ANTIBACTERIAL BIODEGRADABLE Mg-Ag ALLOYS 25 (2013) 284–298, https://doi.org/10.22203/eCM.v025a20.

[28] H. Hornberger, F. Witte, N. Hort, W. Mueller, Effect of fetal calf serum on the corrosion behaviour of magnesium alloys, Mater. Sci. Eng. B 176 (20) (2011) 1746–1755, https://doi.org/10.1016/j.mseb.2011.07.018.

[29] J. Gonzalez, R.Q. Hou, E.P.S. Nidadavolu, R. Willumeit-Römer, F. Feyerabend, Magnesium degradation under physiological conditions – best practice, Bioact. Mater. 3 (2) (2018) 174–185, https://doi.org/10.1016/j.bioactmat.2018.01.003.

[30] S. Fajardo, C.F. Glover, G. Williams, G.S. Frankel, Electrochimica acta the source of anodic hydrogen evolution on ultra high purity magnesium, Electrochim. Acta 212 (2016) 510–521, https://doi.org/10.1016/j.electacta.2016.07.018.
[31] G. Williams, N. Birbilis, H.N. Mcmurray, Electrochemistry Communications the source of hydrogen evolved from a magnesium anode, Electrochem. Commun. 36 (2013) 1–5, https://doi.org/10.1016/j.elecom.2013.08.023.
[32] M. Curioni, Electrochimica Acta the behaviour of magnesium during free corrosion and potentiodynamic polarization investigated by real-time hydrogen measurement and optical imaging, Electrochim. Acta 120 (2014) 284–292, https://doi.org/10.1016/j.electacta.2013.12.109.
[33] Y. Gao, et al., Effect of stress on corrosion of high-purity magnesium in vitro and in vivo, Acta Biomater. 83 (2019) 477–486, https://doi.org/10.1016/j.actbio.2018.11.019.
[34] N.T. Kirkland, J. Lespagnol, N. Birbilis, M.P. Staiger, A survey of bio-corrosion rates of magnesium alloys, Corrosion Sci. 52 (2) (2010) 287–291, https://doi.org/10.1016/j.corsci.2009.09.033.
[35] F. Witte, N. Hort, F. Feyerabend, C. Vogt, "Magnesium (Mg) corrosion: a challenging concept for degradable implants," *Corros*, Magnes. Alloy. (2011) 403–425, https://doi.org/10.1533/9780857091413.3.403.

My curriculum vitae does not appear in the electronic version of my paper for reasons of data protection

Publication list

1. **Yuqiuhan Zhang**, Tycho Zimmermann, Wolf-Dieter Mueller, Frank Witte, Florian Beuer, Andreas Schwitalla. Exploring the degradation behavior of MgXAg alloys by in vitro electrochemical methods. Bioactive Materials, 2021, ISSN 2452-199X, https://doi.org/10.1016/j.bioactmat.2021.05.044.

   Impact Factor (2021): 14.593

2. Zimmermann T, Hort N, **Zhang Y**, Müller WD, Schwitalla A. The Video Microscopy-Linked Electrochemical Cell: An Innovative Method to Improve Electrochemical Investigations of Biodegradable Metals. Materials (Basel). 2021 Mar 25;14(7):1601. doi: 10.3390/ma14071601.

   Impact Factor (2019): 3.623

3. **Zhang Y**, Liu J, Zhang P, Clinical evaluation of CEREC all-ceramic inlays and resin restoration of Posterior Teeth Class II Cavity. The Journal of Practical Medicine. 2016,32(23):3853-3855. DOI:10.3969

Acknowledgements

First of all, I would like to offer my sincere appreciation to everyone who has supported me during my doctorate studies. My heartfelt appreciation goes to Prof. Dr. Wolf-Dieter Müller, my supervisor, for providing this invaluable opportunity and invited me to participate in this excellent project. His enlightened counsel has always illuminated the road of scientific study that is dominated by the unknown and guided me in the correct direction whenever I needed it. I'd also want to express my gratitude to Prof. Dr. Andreas Schwitalla and Dr. Tycho Zimmerman for their support with my doctorate research. Without their continuous advice and guidance, I would not have been able to achieve my goals.

My special thanks Prof. Dr. Florian Beuer, Dr. Franziska Schmidt and Frau Christiane Schöpf, for the pleasant collaboration and their great help in technical supporting and guidance. Without their passionate participation and input, the research could not have been successfully conducted.

My wonderful colleagues and friends Yiqiao Wang, Lucia Nascimento and Haohan Zou thank you for offering support and helping me out of trouble no matter in lab or in life over the past three years. It was such a great time to work in a lab filled with so many excellent colleagues and friends.

Last but not least, my deepest gratitude goes to my beloved families and friends, especially my mother Weihong Zhang and my husband Jürgen Rau. Thank you for always upholding my decision, for sharing my sorrow and joy throughout this journey. I am truly grateful for the days in Berlin and the unforgettable memories here.